Annu. Rev. Biochem. 2003. 72:813–850
doi: 10.1146/annurev.biochem.71.110601.135450

THE STRUCTURAL BASIS OF LARGE RIBOSOMAL SUBUNIT FUNCTION

Peter B. Moore [1, 2] and Thomas A. Steitz [1, 2, 3]
[1]Departments of Molecular Biophysics and Biochemistry, and [2]Chemistry, Yale University, and [3]Howard Hughes Medical Institute, New Haven, Connecticut 06520; email: moore@proton.chem.yale.edu, eatherton@csb.yale.edu

Key Words ribosomes, crystallography, peptidyl transferase, antibiotics

■ **Abstract** The ribosome crystal structures published in the past two years have revolutionized our understanding of ribonucleoprotein structure, and more specifically, the structural basis of the peptide bonding forming activity of the ribosome. This review concentrates on the crystallographic developments that made it possible to solve these structures. It also discusses the information obtained from these structures about the three-dimensional architecture of the large ribosomal subunit, the mechanism by which it facilitates peptide bond formation, and the way antibiotics inhibit large subunit function. The work reviewed, taken as a whole, proves beyond doubt that the ribosome is an RNA enzyme, as had long been surmised on the basis of less conclusive evidence.

CONTENTS

INTRODUCTION 814
Background 814
The Scope of This Review 816
RIBOSOME CRYSTALLOGRAPHY 816
Crystals 816
Crystallography 818
THE ARCHITECTURE OF THE LARGE RIBOSOMAL SUBUNIT 825
RNA Structure in the Large Subunit 826
Proteins of the Large Subunit 831
THE STRUCTURAL BASIS OF LARGE SUBUNIT ACTIVITY 836
Investigating the Enzymatic Activity of the Peptidyl Transferase Center 837
The Polypeptide Exit Tunnel 842
Antibiotics Targeting the Large Subunit 846

INTRODUCTION

Background

The last step in the gene expression pathway, protein synthesis, is executed by a formidable cellular apparatus. In addition to messenger RNAs for every protein currently in production, each cell contains transfer RNAs for (almost) every amino acid it uses to make protein, aminoacyl tRNA synthetases to charge those tRNAs, an array of facilitating protein factors, and finally ribosomes, the massive enzymes that catalyze mRNA-directed protein synthesis.

Elucidation of the chemical basis of protein synthesis has been a goal of biochemists for half a century. In its pursuit, crystallographers have determined the structures of many of the macromolecules involved. The crystal structures obtained for yeast phenylalanine tRNA in the 1970s were the first fruit of this enterprise (1, 2), and over the years many other important structures have been obtained, e.g., all but one of the aminoacyl tRNA synthetases and many of the protein synthesis factors. Long sought, but missing until 2000, were atomic resolution structures for the ribosome and its subunits. The crystal structures of the ribosomal subunits that have recently been determined are the subject of this review.

THE ROLE OF THE RIBOSOME IN PROTEIN SYNTHESIS Functionally, ribosomes are polymerases. Like DNA polymerase and RNA polymerase, they catalyze the synthesis of biopolymers of a single chemical class, and the sequence of the specific member of that class a ribosome makes is determined by its interaction with a nucleic acid template. The substrates ribosomes consume are aminoacyl tRNAs, their products are proteins, and their templates are messenger RNAs.

There are three binding sites for tRNA on the ribosome: an A site, to which aminoacyl tRNAs are delivered in an mRNA-directed fashion, a P site where peptidyl tRNAs reside, and an E site through which deacylated tRNAs pass as they are released from the ribosome (3). Nascent polypeptides are elongated by a cyclic process that starts with a molecule of mRNA bound to the ribosome, a deacylated tRNA in the E site, a peptidyl tRNA in the P site, and a vacant A site. In the first step, an aminoacylated tRNA whose anticodon is complementary to the mRNA codon presented in the A site is delivered to the ribosome by a protein factor that in prokaryotes is called EF-Tu, and the deacylated tRNA in the E site leaves the ribosome. Once delivery has occurred, the peptide esterified to the 3′-terminal A of the P-site bound tRNA is transferred to the amino group of the amino acid esterified to the 3′ terminal A of the tRNA in the A site, which elongates the nascent peptide chain by one amino acid. During the final step in the cycle, translocation, the deacylated tRNA in the P site moves to the E site, the peptidyl tRNA in the A site migrates to the P site, and the ribosome moves down the mRNA, in the 3′ direction, by 1 codon. In prokaryotes, translocation is

catalyzed by a protein factor called EF-G. Once translocation has occurred, the ribosome can accept the next aminoacyl tRNA.

The ribosomes of all species are a 1:1 complex of two subunits of unequal size, the larger being about twice the mol wt of the smaller. During the initiation phase of protein synthesis, subunits are recruited from the pool of dissociated subunits in the cell with the aid of initiation factors. The product of these interactions is a ribosome with a mRNA bound so that the first codon in the message and the corresponding aminoacyl tRNA occupy the P site. Termination occurs when an elongating ribosome encounters a stop codon, which is a codon for which no cognate tRNA exists. Ribosomes stalled at stop codons are recognized by termination factors, which promote the hydrolysis of the ester bond linking the now completed polypeptide to its tRNA, the release of the bound mRNA, and the return of subunits to the cellular pool. Unlike the elongation cycle discussed above, which is effectively the same in all organisms, the mechanism of both initiation and termination differs substantially among kingdom to kingdom.

RIBOSOME STRUCTURE AT LOW RESOLUTION The two subunits of the ribosome perform distinctly different functions during protein synthesis. The small ribosomal subunit programs protein synthesis; it binds mRNA and mediates the interaction between mRNA codons and tRNA anticodons. The large subunit takes care of production; it contains the peptidyl transferase site, the site at which peptide bonds are formed. Consistent with their functions, the small subunit interacts with the anticodon-containing ends of tRNAs, and the large subunit interacts primarily with their CCA termini. There is an A site, a P site,and an E site on both subunits. Both subunits interact with the protein factors that facilitate ribosome function, and intersubunit interactions are important in all phases of protein synthesis.

The mol wt of the ribosome ranges from about 2.5 $x10^6$ in prokaryotes to about 4.5 $x10^6$ in higher eukaryotes, and the typical ribosome is roughly two-thirds RNA and one-third protein. The large subunit of the prokaryotic ribosome sediments at about 50S, and it contains one large RNA (23S rRNA), one small RNAS (5S rRNA), and about 35 different proteins, most of them in single copy.

The overall shape of the ribosome was determined by electron microscopy over 25 years ago (4) [see also (5)]. At ~40 Å resolution, the large subunit is (crudely) a hemisphere about 250 Å in diameter with three projections protruding radially from the edge of its flat face, a large one in the middle (the central protuberance), and two smaller ones at roughly 2 o'clock and 10 o'clock relative to the central protuberance. The central protuberance includes 5S rRNA and its associated proteins (6). Looking at the flat face of the subunit with its central protuberance up, the so-called crown view, the right protuberance includes ribosomal proteins L7/L12, and the left protuberance contains ribosomal protein L1 (7, 8).

Around 1995, the resolution of electron microscopic density maps of the ribosome improved dramatically as a consequence of the perfection of single particle image reconstruction techniques that could be applied to micrographs of ribosomes embedded in vitreous ice (9, 10). In addition to better delineating the morphology of the ribosome, these improved images proved that the large subunit contains a tunnel that runs from roughly the middle of its flat face to the side away from the small subunit in the 70S ribosome, as earlier electron microscopic studies had suggested (11–13, 13a). They also demonstrated that the peptidyl transferase site is located at the end of the tunnel closest to the small subunit in the ribosome (14–17).

The Scope of This Review

The first papers describing atomic structures of ribosomes derived from high resolution X-ray studies that appeared in August 2000, and since then many more have been published. The currently known structures include a 2.4 Å resolution structure of the large subunit from *Haloarcula marismortui* (18), a 3.0 Å resolution structure (19), and a 3.2 Å resolution structure (20) of the small subunit from *Thermus thermophilus*, and a 3.1 Å resolution structure of the large subunit from *Deinococcus radiodurans* (21). In addition, there are numerous structures of complexes of low mol wt substrate, inhibitor and antibiotic ligands bound to these ribosomal subunits, as well as a model of the 70S ribosome from *T. thermophilus* with mRNA, tRNA, and tRNA analogs bound derived from a 5.5 Å resolution electron density map (22).

This chapter begins with an account of how the crystal structures of ribosomes were determined, and it concludes with a review of the information that has emerged that is limited to the large subunit because it is impossible to do justice to both subunits and the 70S ribosome in a single review of this format. Additional information can be found in reviews that have appeared elsewhere in the last two years, e.g., (23–28).

RIBOSOME CRYSTALLOGRAPHY

The year the structure of the large ribosomal subunit from *H. marismortui* was published, it was the largest structure of an asymmetric assembly determined at atomic resolution by about a factor of 4. Ribosomes were, and still remain, challenging targets for crystallographic investigation.

Crystals

Crystals that diffract to resolutions of ~3.5 Å, or better, are the *sine qua non* for macromolecular crystal structure determination. The first three-dimensional crystals of ribosome subunits were grown in the laboratory of H.G. Wittman in 1980 by Yonath et al. from the 50S subunits of *Bacillus*

stearothermophillus (29). Although they diffracted only to low resolution, their existence suggested that X-ray studies of the ribosome might be possible and motivated the search for better crystals. The crystals of 30S subunits (and also 70S ribosomes) from *T. thermophilus*, first prepared in Pushchino in 1987 (30) and in Berlin at about the same time (31), were the progenitors of those that yielded structures, but they too diffracted only to 10–12 Å resolution (32, 33). Likewise, the crystals of the large ribosomal subunit of the archeon, *H. marismortui*, diffracted poorly when first grown in Berlin in 1987 (34) but were gradually improved, and by 1991 crystals that diffracted to 3 Å resolution had been obtained (35). The existence of these crystals showed that an atomic structure was in principle possible, but not until a method could be found for the phasing of diffraction patterns.

Although the *H. marismortui* 50S crystals diffracted well, they had some serious flaws. A number of their defects have been described by Yonath and coworkers (36). They include ". . . severe nonisomorphism, high radiation sensitivity, . . . nonuniform mosaic spread, uneven reflection shape, and high fragility." Later Harms et al. (37) pointed out other problems, ". . . the unfavorable crystal habit (plates, made of sliding layers, reaching typically up to 0.5 mm^2 with an average thickness of a few microns in the direction of the *c* axis), and variations in the *c* axis length (567–570 Å) as a function of irradiation."

The Yale group discovered yet another problem, crystal twinning (38). Depending on how these crystals are handled after they have grown, a 10 Å shift in the relative positions of subunits may occur that changes their space group symmetry from orthorhombic, $C222_1$, to monoclinic, $P2_1$, with almost no alteration in unit cell dimensions, or crystal cracking, and, surprisingly, no alteration in the symmetry of the crystal's diffraction pattern. The reason for the latter is that the direction of the packing shift varies randomly from one mosaic block to the next within a crystal, and hence crystals in which it has occurred are twinned.

These crystal pathologies were all eventually overcome. Crystal to crystal isomorphism was improved, twinning was suppressed using an appropriate stabilizing solution, and crystal thickness was increased to between 0.1 and 0.2 mm using a reverse extraction procedure for crystal growth that also increased crystal strength and singularity (18). The result was extension of the maximum resolution of the diffraction patterns of these crystals to 2.2 Å.

The reports of the two groups that solved the structure of the 30S subunit from *T. thermophilis* indicated that the crystallization issues they overcame were less dramatic, albeit no less essential for success (39, 40). A full account of how the 70S crystals were grown that were used to obtain the 5.5 Å resolution structure referred to above has yet to be published. Interestingly, the paper that reports the crystal structure of the *D. radiodurans* large subunit structure is also the first report of the existence of the corresponding crystals (21).

Crystallography

Although crystallographic technology was perhaps not up to the task of ribosome structure determination when the first crystals were grown in 1980, 10 years later, when crystals that diffract to high resolution had been obtained, all the X-ray and computational technologies required were in place: synchrotron radiation, crystal freezing, phosphorimaging detection, and the requiste computers and programs. The strategy for solving the structure of the large ribosomal subunit from *H. marismortui*, in brief, was to begin at extremely low resolution using data from 100 to 16 Å resolution, where the scattering power of heavy atom cluster compounds is enhanced by up to 100-fold, and to check the validity of heavy atom positioning with phases derived from a 20 Å resolution cryo-electron microscopy (EM) reconstruction. This led to the first ribosome electron density map, at 9 Å resolution, that showed density corresponding to recognizable macromolecular features (46). This map provided the means to proceed to progressively higher resolution. A more complete description of the trials and tribulations that led from the first crystals to the first atomic structure follows.

X-RAY SOURCES AND COMPUTERS While it is certainly the case that the ribosome crystal structures could not have been solved without the use of synchrotron X-ray sources, progress was never impeded by the lack of synchrotron beam lines of appropriate quality. The X-ray data used in the Yale 5 Å resolution map of the *H. marismortui* 50S subunit, for example, were measured on a bending magnet beamline at Brookhaven National Lab, X12B, which produces what is by today's standards a quite weak X-ray beam, and data for a 3 Å resolution map that allowed complete interpretation of the electron density corresponding to 23S rRNA were measured at beamline X-25 using a phosphorimaging plate detector.

Similarly, ribosome crystallography was not hampered by the lack of computational tools any more than virus crystallography had been. The supercomputers available in the early 1990s would have sufficed to do all the computation needed to solve ribosome crystal structures, and by the late 1990s all of the computation required could be executed in a few days on a high-end workstation.

DETECTORS Because the unit cell dimensions of the virus crystals are comparable to those of ribosome crystals, and because the first virus structures were solved in the late 1970s and 80s, it could be argued that the determination of ribosome crystal structures was technically feasible decades before it was accomplished. However, the low quality of the data obtainable using film-based data collection methods, which were limited by the high background and the narrow range of linearity, would have made it extremely difficult, since very small isomorphous and anomalous diffraction intensity differences had to be measured with high accuracy. The limitations of film were far less important for the determination of virus structures because the internal symmetry of viruses makes it possible to use powerful averaging methods for improving electron density maps.

Both charge coupled device (CCD) and phosphorimaging plate X-ray detectors, which came into use in the 1990s, can measure diffraction data with the requisite accuracy, though the CCD detectors are far faster. The disadvantage of CCD detectors, for ribosome crystallography in the 1990s derived from their small size. Even the CCD detector available at ID19 at the Advanced Photon Source (APS) at Argonne National Laboratory, which was exceptionally large, limited data collection from the *H. marismortui* large subunit crystals by the Yale group to under 2.4 Å resolution. The speed of data collection was stunning, however. More than 6 million reflections were measured in a few hours, which is a data collection rate about 10^5 times faster than could be achieved in the 1960s using state of the art laboratory equipment and crystals of molecules 50 times smaller.

CRYSTAL FREEZING The development of ways to freeze crystals and to collect data from them at -140°C was one of the most important developments in macromolecular crystallography of the last decade or so because it enabled the use of the high intensity synchrotron X-ray sources that were necessary for solving the structure of the ribosome and for the rapid solving of other protein and nucleic acid structures. At room temperature, the crystals of all biological macromolecules wither due to radiation damage when exposed to the intense and tunable X-ray beams that are necessary for crystallographic studies of large structures and for MAD phasing. The in-beam lifetime of crystals is greatly enhanced if they are flash frozen before exposure and remain frozen during data collection.

The first successful X-ray diffraction experiments done with frozen crystals were executed in 1970 by Rossmann and colleagues using crystals of lactate dehydrogenase that had been immersed in sucrose solutions (40a). Because the benefits of freezing were not commensurate with the technical difficulties involved at the time, the method did not come into general use. Nearly two decades later, after the development of synchrotron X-ray sources had brought the issue of radiation damage to the fore, Hope devised a method for flash-freezing protein crystals in liquid nitrogen (40b) and then, in collaboration with Yonath, demonstrated its efficacy using ribosome crystals (41). Ribosome crystals are so sensitive to radiation damage that data cannot be collected from any of them effectively unless they are frozen, and even when frozen, some are still significantly damaged by short exposures to synchrotron radiation.

PHASING STRATEGIES Once crystallographically suitable crystals have been obtained, the major barrier to solving any crystal structure is determining the phases that are associated with its X-ray diffraction amplitudes. Although the ribosome is not larger than the viruses whose structures were solved in the late 1970s and early 1980s, the lack of internal symmetry in the ribosome precluded the use of averaging methods for phase (map) improvement that have been so essential for the determination of virus structures. The only phasing method that

could be used for the ribosome was heavy atom-multiple isomorphous replacement appropriately combined with anomalous scattering.

To obtain measurable diffraction intensity changes from heavy atom derivatized crystals of such a large asymmetric assembly, either a large number (50 to 100) of single heavy atoms or a smaller number (1 to 10) of heavy atom cluster compounds need to be bound and their positions in the crystal located. The crucial step in the process of obtaining an interpretable electron density map is determining the positions of the bound heavy atoms, and when the number of heavy atom sites is large, it is difficult to accomplish using standard difference Patterson methods.

The strategy used to solve the phasing problem for ribosome crystals involved multiple steps (18, 38, 46). The objective of the initial step was to correctly determine the positions of heavy atom cluster compounds at very low resolution (20Å), which were then used to produce reliable phases to 5 Å resolution. These low resolution phases were then used to locate the positions of heavy atoms in derivatized crystals containing a large number of single-atom heavy atom molecules. The difference Fourier methods enabled by low resolution phases are effective for locating large numbers (~100) of heavy atom positions. Once this was achieved, phasing could then be extended to high resolution. Phases to 20 Å resolution were obtained by two methods: isomorphous replacement using heavy atom cluster compounds and molecular replacement using electron microscopic images. All of the de novo ribosome structure determinations reported so far have used similar phasing strategies.

Heavy atom cluster compounds are particularly powerful at very low resolutions (out to 20 Å) because they produce extraordinarily large diffraction intensity changes. One of the cluster compounds used to prepare isomorphous derivatives of *H. marismortui* large subunit crystals, for example, contained 18 tungsten atoms. At 20 Å resolution the intensity change, $|F|^2$, produced by one W18 molecule bound per asymmetric unit approximates what would be observed if 324 ($= 18^2$) tungsten atoms were bound at random positions. It scatters like a super heavy atom containing 18x74 electrons. Not only is the intensity change produced by one to five such cluster compounds easy to observe, but the low resolution difference Patterson maps that emerge are easy to interpret. A derivative containing one to five single heavy atoms would generally not produce measurable intensity changes with the ribosome. It should be noted, however, that the intensity changes produced by heavy atom cluster compounds fall off very rapidly with resolution due to interference effects, and at resolutions approaching that of radius of the cluster compound and beyond (~ 10 Å), the changes will be less than that of the same number of heavy atoms bound at random sites. Even if cluster compound data do not yield high resolution phases, the low resolution phase information provided can be used to obtain the positions of multiple site, single heavy atom compounds by difference Fourier methods, which will work with even more than 100 sites.

Electron density maps derived by electron microscopy can also be used to obtain very low resolution phases for X-ray diffraction patterns and are very useful for validating the positions of heavy atom clusters that have been determined by other means. In the 1970s, Harrison and coworkers used the three-dimensional images of viruses derived from electron micrographs of negatively stained particles to phase viral X-ray diffraction patterns at low resolution by molecular replacement and used these phases to locate heavy atoms (42). The three-dimensional cyro-EM images of ribosomes produced by the mid-1990s (see above) were of a substantially higher quality and resolution and were useful in producing phases to validate heavy atom positions (46).

SOLVING THE STRUCTURE OF THE *H. MARISMORTUI* LARGE SUBUNIT The first attempts to phase ribosome diffraction patterns were made by the Yonath group using heavy atom cluster compounds, but the electron density maps that resulted did not show the continuous density features characteristic of RNA and protein (36, 37, 43, 44), and it appears that the subunit packings inferred from solvent flatterned maps presented for both the *H. marismortui* large subunit and the *T. thermophilus* small subunit (45) were incorrect because they are not the same as those deduced for the same crystals subsequently (18, 19, 46).

The first heavy atom-derivatized ribosome crystal in which heavy atom positions were successfully determined was obtained by soaking a cluster compound containing 18 tungsten atoms into crystals of the *H. marismortui* large ribosomal subunit (46). Fortuitously, this compound binds to those crystals predominantly at a single location, which simplified determination of its position. It was located initially by difference Patterson methods, and its location was confirmed later by a difference electron density map computed using low resolution X-ray diffraction amplitudes and phases obtained by molecular replacement. The model used for molecular replacement was a 20 Å resolution cryo-electron microscopic reconstruction of the *H. marismortui* 50S subunit provided by Frank and colleagues. By far the largest feature in the difference map that emerged was a 13 σ peak at the position predicted from difference Patterson maps that was 6 σ higher than the next highest peak, which turned out to be that of another site with lower occupancy (46). Molecular replacement was also used to understand the twinning problem discussed above.

The first electron density map published of any ribosome or ribosomal subunit that showed features clearly interpretable in molecular terms was a 9 Å resolution map of the *H. marismortui* large ribosmal subunit (Figure 1*a*), which included rods of density of the appropriate size that show the right handed but irregular twist characteristic of RNA duplex (46).

Because the heavy atom cluster compound derivatives obtained for *H. marismortui* large subunit crystals had little phasing power beyond about 5 Å resolution, experimental phase extension depended on derivatives prepared using single-atom, heavy-atom compounds such as osmium pentamine and iridium hexamine. The positions of the more than 100 osmium and iridium atoms bound

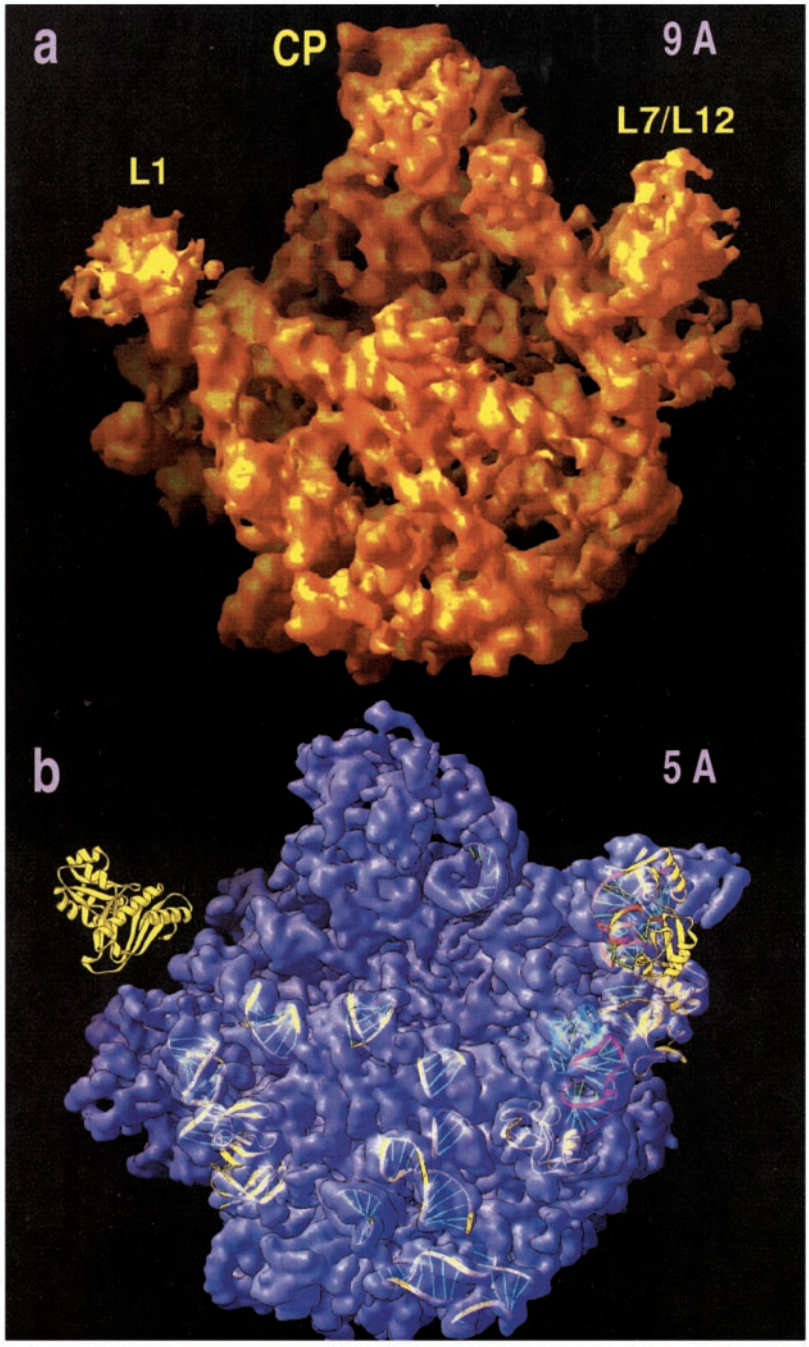
a
CP
9 A
L7/L12
L1
b
5 A

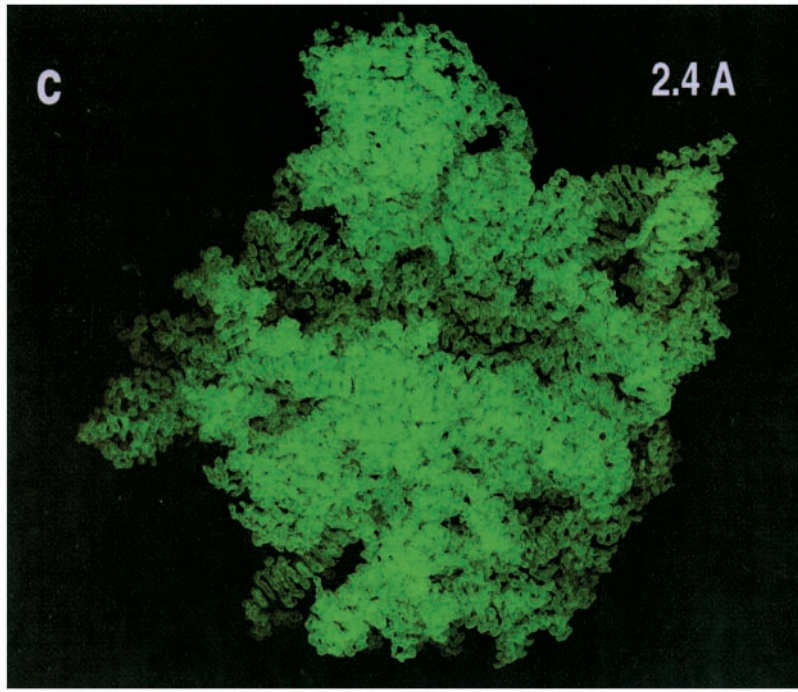

Figure 1 Continued

in the unit cell were located using difference Fourier maps computed employing the 5 Å resolution phases previously determined. Only at this stage in the investigation, when the structure was already solved in principle, did it become necessary to collect data using high intensity beam lines. The high resolution data produced by two trips to high brilliance beam lines resulted finally in a 2.4 Å resolution electron density map of the *H. marismortui* large ribosomal subunit.

The unusually high quality of the final, experimentally phased electron density map of the *H. marismortui* large subunit is due to several factors. It is attributable in part to the well-collimated, high intensity, 80 μ diameter X-ray beam used to collect data at beam line ID19 and the small pixel size and relatively large size of the CCD detector used, which made it possible to collect very accurate data.

←

Figure 1 The appearance of the large ribosomal subunit from *H. marismortui* in electron density maps at different resolutions. The subunit is shown in the crown view at (*a*) 9 Å resolution (46), (*b*) 5 Å resolution (38), and (*c*) 2.4 Å resolution (18). CP designates the central protuberance. The L1 stalk, which is visible at low resolution, disappears as resolution improves. [Reproduced with permission from (46a).]

The solvent flipping density modification (46b) program as implemented in the Crystallography and NMR System (CNS) program package proved remarkably effective at improving both the quality and resolution of the heavy atom phased maps (Figure 1*c*).

SOLVING THE STRUCTURE OF THE SMALL SUBUNIT The first clear indication that a structure would soon be obtained for the small subunit was the partially interpreted 5.5 Å resolution electron density map of the 30S subunit from *T. thermophilus* presented by Ramakrishnan and colleagues at a meeting in the summer of 1999 (47) and published soon thereafter (48). A year later, the same group published a fully interpreted structure for the 30S subunit at 3.05 Å resolution (19). Their structure appeared shortly after a paper from the Yonath group describing a less accurate and less completely interpreted 3.3 Å resolution electron density map of the small subunit (40). The differences between the two structures have been resolved in favor of the Ramakrishnan structure (20). Initial low-resolution phases for both of these 30S subunit structures were obtained using heavy atom cluster compounds (39, 40). The extension of the phasing of the Ramakrishnan 30S map to 3 Å resolution depended on data from multiple site, single, heavy atom derivatives (39) including good anomalous scattering measurements. Remarkably, one of the tungsten cluster compounds employed by the Yonath group in their studies of the small subunit studies contained one well ordered site that produced useful phasing extending to 3.3 Å resolution (40).

OTHER RIBOSOMAL STRUCTURES The crystal structure of the 70S ribosome derives from a phasing process that also began at very low resolution with molecular replacement using EM-derived ribosome images to assist in heavy atom locations in derivatives that ultimately extended the resolution to 5.5 Å (22, 50). As pointed out earlier, a resolution of 5.5 Å is well below that needed for the independent interpretation of electron density maps. Nevertheless, most of the sequence of 16S rRNA was fit into the electron density of the small subunit part of the map, albeit less accurately, without reference to other structures, and the large subunit electron density was interpreted using the Yale *H. marismortui* large subunit structure as a guide. At this resolution, the positions of bases cannot be seen, and 50S proteins of unknown structure could not be solved. However, the resulting 70S structure provides important information about the conformational differences between free subunits and subunits in 70S couples, the structures of the connections between the two subunits, and the placement of mRNA and tRNAs on the intact ribosome.

In the last three years, the Yonath group has obtained structures for two different large ribosomal subunits. The first was a 3.6 Å resolution structure of the large subunit from *H. marismortui* derived from crystals similar to those used by the Yale group, but it was stabilized in a buffer containing more K^+ and less Na^+ (52). This structure, which was obtained from a map calculated using a phasing strategy that combined molecular replacement using the Yale structure

and anomalous scattering from isomorphous derivatives, is reported to differ from the Yale structure in several ways. First, the Yale structure is reported to be systematically somewhat larger. Second, the Yonath subunit includes structures for the 23S rRNA sequences omitted from the Yale structure because of their low visibility. Third, the conformations found for some of the proteins are different. Because a full description of this structure has not appeared and its coordinates have not been released, it is impossible to comment on it further. However, since the *D. radiodurans* 50S subunit and the large subunit of the 70S structure are the same size as the Yale *H. marismortui* structure and homologous proteins have similar conformations, it is unclear why the *H. marismortui* 50S structure reported by the Yonath group is so different.

The Yonath group has also solved the structure of the 50S subunit from *D. radiodurans* (21). Phases were obtained initially by molecular replacement using the Yale *H. marismortui* structure and then improved using heavy atom isomorphous replacement and anomalous scattering data. The latest version of this structure (PDB # 1LNR) has been refined to a free R of 27.9%. However, for the purposes of refinement, the atoms of each nucleotide were divided into 2 groups, a ribose group and a base + phosphorus group, which were assigned independent B-factors. The B-factor variations in 1LNR between groups of atoms within single nucleotides, and from one nucleotide to the next are too large to be physically meaningful, and their existence indicates that the structure is not fully refined. Refinement limitations may be the root source of the controversy that has arisen about the structures of some of the proteins in earlier releases of this structure (53, 54).

THE ARCHITECTURE OF THE LARGE RIBOSOMAL SUBUNIT

Below we discuss the structure and function of the large subunit, using the Yale *H. marismortui* large subunit crystal structure (PDB # 1JJ2) as the standard. The other structures of the large subunit that have been determined are the large subunit part of the *T. thermophilus* 70S ribosome (22), the *D. radiodurans* large ribosomal subunit (21), and the *H. marismortui* large ribosomal subunit examined at higher K^+ concentrations (52). These structures are similar but not identical in every detail, and unfortunately, it is hard to interpret the sources of the differences. The refinement problem evident in the *D. radiodurans* structure raises questions about its coordinate accuracy. The 70S-derived large subunit structure is not fully independent because it was derived originally from the standard *H. marismortui* structure, and the 5.5 Å resolution of the map is not sufficient to enable a reliable modeling of RNA differences or interpretation of the uniquely eubacterial proteins, which are not fully interpreted. In addition, because *H. marismortui* is archaeal, and the other two species are eubacterial, there are substantial sequence differences in both RNA and protein. Finally, both

of the eubacterial structures were determined at moderate ionic strength, although the standard structure, which derives from an extreme halophile, was obtained from crystals in which the ionic strength is about 3 M.

One difference between the standard *H. marismortui* structure and the others is that all the latter include many of the parts of the large ribosomal subunit omitted from the standard structure because of local disorder. The visibility of these components in the high-K^+ *H. marismortui* structure is particularly puzzling. The Yale group has determined the structure of *H. marismortui* large subunit crystals in which the predominant cation is K^+, not Na^+, and finds the visibility of these regions unaffected (J.L. Hansen, unpublished results). In thinking about this problem, it should not be forgotten that the lower the resolution of an electron density map, the easier it is to visualize its less well ordered regions. The features missing from the Yale structure at 2.4 Å resolution were visible in its 9 Å resolution electron density maps (46), and the high-K^+ *H. marismortui* structure was determined at 3.6 Å resolution.

All of these structures support two important conclusions. First, the shape of the large subunit, like that of the small ribosomal subunit, is determined by its RNA; pictures of the large subunit drawn with its proteins omitted look just like the pictures obtained when they are included. Second, the large subunit is monolithic. Except for its two lateral protuberances, which are flexibly attached to the rest of the subunit by single RNA stems, the object has no obvious morphological subdivisions.

RNA Structure in the Large Subunit

The secondary structure of 23S rRNAs has been investigated by comparative sequence analysis since the early 1980s (55, 56). The crystal structures of the large subunit prove that the secondary structure model obtained by sequence comparisons was remarkably accurate. Better still, the overwhelming majority of its errors proved to be pairings that exist but were omitted from the model because they had not been detected, rather than pairings included in the model that do not exist.

DOMAINS IN 23S rRNA Like all large RNAs, 23S rRNA secondary structure is discussed in terms of domains, a concept that also works well in three dimensions for 16S rRNA and many other RNAs, but it is less useful here. RNA secondary structure can be represented as a succession of stem/loops; a domain is a stem/loop that has a loop so large it contains stem/loops of its own. Implied in the use of the word "domain" to describe such structures is the notion that they will fold properly in isolation. There are 11 independent stem/loops in the secondary structure of 23S rRNA, 6 of which meet the domain definition. The remaining five are stems capped by loops too small to contain stem/loops of their own. In addition, as is the case with many other large RNAs, the 5′ and 3′ terminal sequences of 23S rRNA form a helix that, formally, makes the entire molecule a single domain. Nevertheless, 23S rRNAs are deemed to consist of six

domains, one for each of the stems that has a hypertrophied loop, and its five simple stem/loops are considered to be components of the complex stem/loops they adjoin (55). The assignment of the simple stem/loops to domains that resulted did not work out in every case. For example, helix 25 of 23S rRNA, which is one of the simple stem/loops, has been considered to be part of domain 1, but its interactions in the three-dimensional structure of the ribosome clearly indicate that it belongs to domain 2 (18). 5S rRNA is effectively the large subunit's seventh RNA domain.

There is some evidence that the domains of 23S rRNA can fold autonomously, but there is also reason to believe the significance of these observations is not as deep as it is for the domains of 16S rRNA. Oligonucleotides having sequences corresponding to domains I, IV, and VI of 23S rRNA appear to assume ribosome-like secondary structures independently, and there are indications that their tertiary structures are also native-like in isolation (57–59). In addition, in isolation, all six domains form complexes in vitro with at least some of the proteins that bind to them in the ribosome (60). Nevertheless, as already noted, the large ribosomal subunit is not divided into morphologically distinct domains. The secondary structure domains in 23S rRNA interact extensively with each other in the intact ribosome, and the intimacy of their interdomain interactions are indistinguishable from that of their intradomain interactions.

SECONDARY STRUCTURE MOTIFS IN rRNAs An RNA secondary structure motif is a specific sequence or family of sequences or set of non-Watson-Crick base-base juxtapositions that occurs with an appreciable frequency in RNAs generally and that has a distinctive conformation, independent of context. Prior to 2000, fewer than 10 RNA motifs were known, e.g., the GNRA tetraloop and the bulged G motif (61, 62). Examples of all of the previously known motifs can be found in rRNA.

It seemed possible in 2000 that the enormous increase in the amount of RNA structure known at high resolution embodied in the ribosome crystal structures would lead to the discovery of many new secondary structure motifs. However, only one entirely new motif has emerged so far, the kink-turn (63). A motif found previously in tRNA, the T-loop (64) is now seen to be more generally observed, and a secondary structure feature, the hook-turn (65), has been recognized. The small size of the harvest suggests that our knowledge of RNA secondary structure is close to complete.

Kink-turns, or K-turns, are asymmetric internal loops embedded in RNA double helices (63) (Figure 2). Each asymmetric loop is flanked by C-G base pairs on one side and sheared G-A base pairs on the other, with an A-minor interaction between these two helical stems (Figure 2). A consensus sequence and secondary structure derived from the 9 K-turns in the ribosome have a 3-nucleotide loop and 10 consensus nucleotides out of 15 that predict its presence in at least 5 other RNAs. In three dimensions, the most striking feature of a K-turn is the sharp bend in the phosphodiester backbone of the 3-nucleotide

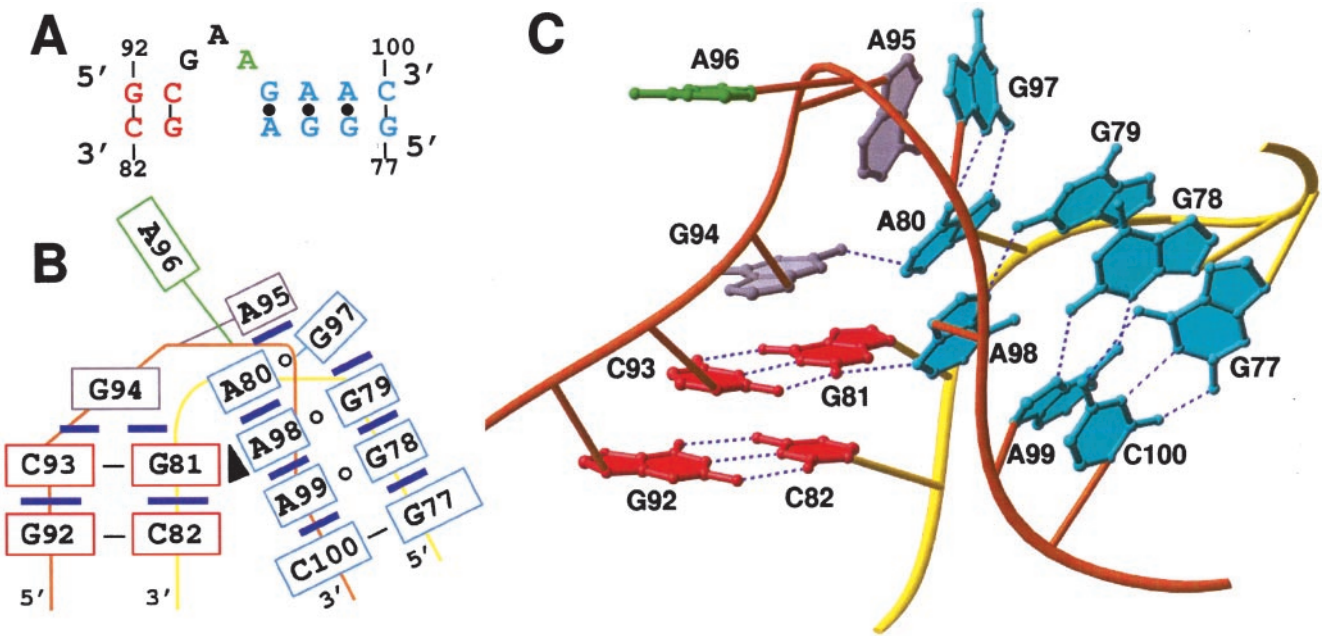

Figure 2 The structure of kink-turn 7 in the 23s rRNA of the *H. marismortui* ribosome. (*a*) The secondary structure of KT-7. The C-stem is red, the NC-stem blue, and the bulged nucleotide is green. (*b*) Base pairing and stacking interactions in KT-7. The black triangle identifies an A-minor interaction. (*c*) KT-7 in three dimensions. The backbone of the kinked strand is orange, and that of the unkinked strand is yellow. Dashed lines indicate hydrogen bonds. [Reproduced with permission from (63).]

bulge that leaves its third base pointing out into solution and results in an ~60° difference in the orientation of the axes of the two flanking helices. Five of the 6 K-turns in the *H. marismortui* large subunit interact with 9 of the 27 proteins visible in that structure, but they interact with proteins of unrelated structures in entirely different ways.

The T-loop motif is a terminal loop structure that has been known for years (64). The TψC-loop of every tRNA adopts that conformation. What had not been previously realized is that T-loops occur in other contexts, e.g., in rRNAs. There is some variation among T-loops, but in RNA secondary structure diagrams, they are usually seven-base loops. The 5′ base of the loop, which is always a U, forms a Hoogsteen pair with the A at the fifth position. That pair stacks on the Watson-Crick pair that terminates the stem, leaving the bases 3′ to that A bulged out. A base from another part of the molecule inserts between the same A and the base at the fourth position.

Hook-turns are found at places where the two strands of a helix are separating to interact with other sequences (65). Their conformations are not determined entirely by local interactions, and their consensus is short enough to make them difficult to identify in secondary structure diagrams so that their status may not quite rise to the level of a bona fide motif. Nevertheless, they tend to follow helices that end with a GC base pair and an AG juxtaposition (65), and in the space of two nucleotides, the direction of the backbone of the strand 3′ to the G changes about 180°. The first nucleotide in the sequence that forms the bend is often an A.

LONG-RANGE INTERACTIONS IN 23S rRNA Prior to the determination of the structure of the ribosome, little was known about long-range RNA-RNA interactions because so few of the RNA structures known were large enough to have tertiary structures. It was understood, of course, that base pairing between remote single stranded bases stabilizes the tertiary and quaternary structure of RNAs, and two tertiary/quaternary structure motifs had been identified: the tetraloop-tetraloop receptor motif (66) and the ribose zipper (67). These interactions all occur in the ribosome.

So far, only one new long-range RNA interaction motif has been discovered: the A-minor motif (68) (Figure 3). This motif was uncovered by examining the reason for the large number of highly conserved A residues in 23S rRNA, particularly in single stranded regions. This motif is termed “A-minor” because it involves the insertion of the smooth minor groove (C2-N3) edges of adenines into the minor grooves of neighboring helices, preferentially at C-G base pairs where they form hydrogen bonds with one or both of the 2′ OHs of those pairs. In the most abundant and presumably most stable type I interaction, the inserted A forms a triple base pair with the G-C having its N3 hydrogen bond to the N3 of the G and its 2′ OH hydrogen bond to the O2 of the C (Figure 3). Less intimate and less abundant A-minor interactions termed types O, II, and III also occur,

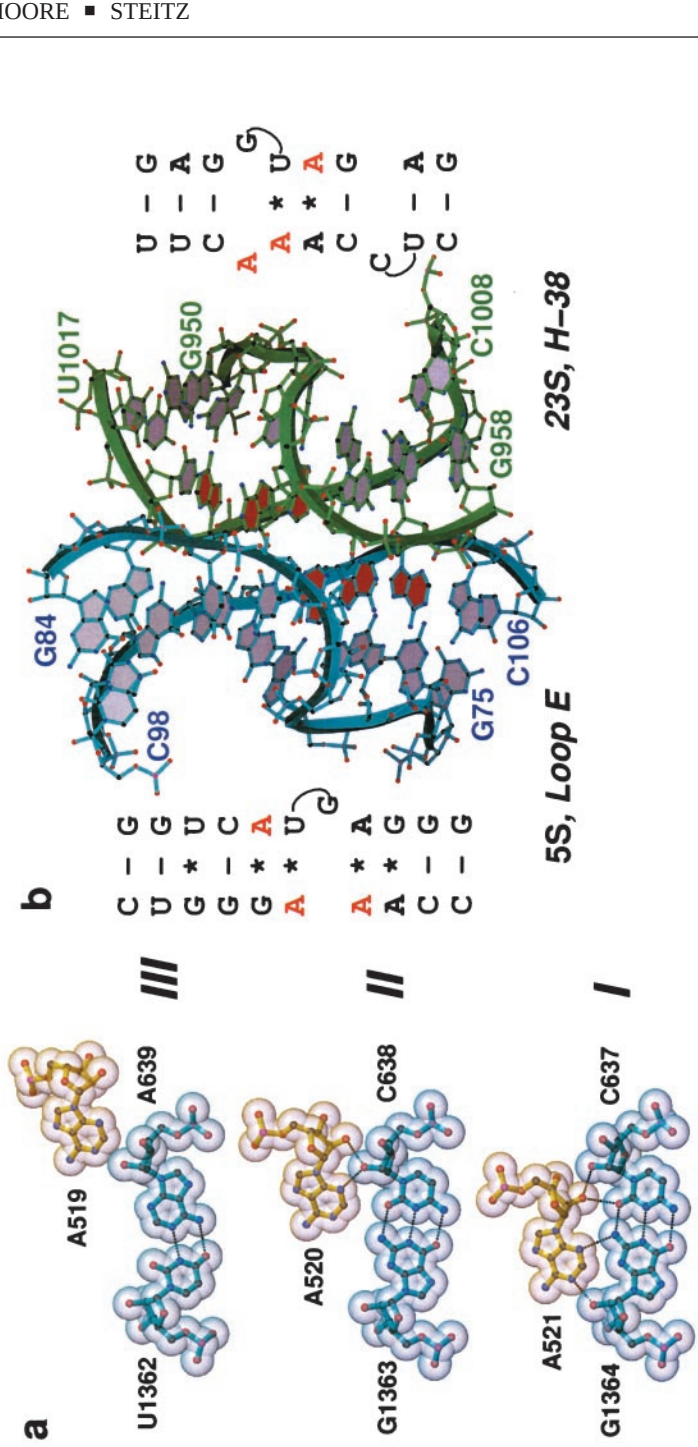
a
A519
A639
U1362
A520
C638
G1363
A521
C637
G1364
III
II
I
b
C — G
U — G
G * U
G — C
G * A
A * U
G
A * A
A * G
C — G
C — G
U — G
U — A
C — G
A A
A * U
G
A * A
C — G
C U — A
C — G
U1017
G950
G84
C98
C1008
G958
C106
G75
5S, Loop E
23S, H–38

usually in sequential association with type I interaction as short runs of As (up to 3), which stack on each other to form what is termed an "A-patch" (68).

These A-minor interactions often involve As in single-stranded regions, but the As in a shared GA pair that is followed by a reverse Hoogsteen UA may also participate because even these paired As are accessible for A-minor interactions (68). The A-minor motif is by far the most abundant tertiary structure interaction in the large ribosomal subunit; 186 adenines in 23S and 5S rRNA are involved compared with about 100 long-range base pairs. As vital structural elements, they are highly conserved; 99 of the 170 A-minor interactions in 23S RNA are greater than 90% conserved across all kingdoms.

In addition to stabilizing specific tertiary structure, A-minor interactions appear to play functionally significant roles in the ribosome. tRNAs are involved in functionally significant A-minor interactions in both the large and small subunits. The 3′-terminal A76 of tRNA molecules bound to both the A site and the P site make type I interactions with 23S rRNA (68, 70). In the small subunits, type I A-minor interactions made by A1492 and A1493 play a critical role in messenger decoding by assuring Watson-Crick pairing between the first and second bases of the codon and the appropriate anticodon (71).

METAL IONS Specifically bound metal ions play an important role in stabilizing the compact tertiary structure of the large 23S and 5S RNA polyanions; these account for the well known capacity of Mg^{2+} ions to stabilize RNA structure. The Yale *H. marismortui* large subunit structure is the only one determined at high enough resolution to allow identification of metal ion interactions with a high degree of confidence. The current structure [PDB# 1JJ2; (63)] includes 88 monovalent cations, 117 Mg^{2+} ions, 22 Cl^- ions, and 5 Cd^{2+} ions. The Cd^{2+} ions included in crystallization buffers replace the Zn^{2+} in the several zinc-finger proteins contained in the *H. marismortui* large subunit (18). Mg^{2+} ions are seen in this structure in regions where the local density of phosphate groups is unusually high, and there they help stabilize structure by neutralizing charge. (D. Klein, T.M. Schmeing, P.B. Moore, and T.A. Steitz, in preparation).

Proteins of the Large Subunit

Following the initial reports on the structures of proteins and their interactions with each other and with rRNA in the large (18, 21) and small (19) subunits,

Figure 3 The A-minor motif. (*a*) Examples of the three most important kinds of A-minor motifs from the 23S rRNA of *H. marismortui*. Types I and II are A-specific. Type III interactions involving other base types are seen, but A is preferred. (*b*) The interaction between helix 38 of 23S rRNA and 5S rRNA in *H. marismortui*. The only direct contact between these two molecules includes six A-minor interactions, involving three As in 23S rRNA and 3 As in 5S rRNA that are symmetrically disposed. Secondary structure diagrams are provided for the interacting sequences. [Reproduced with permission from (68).]

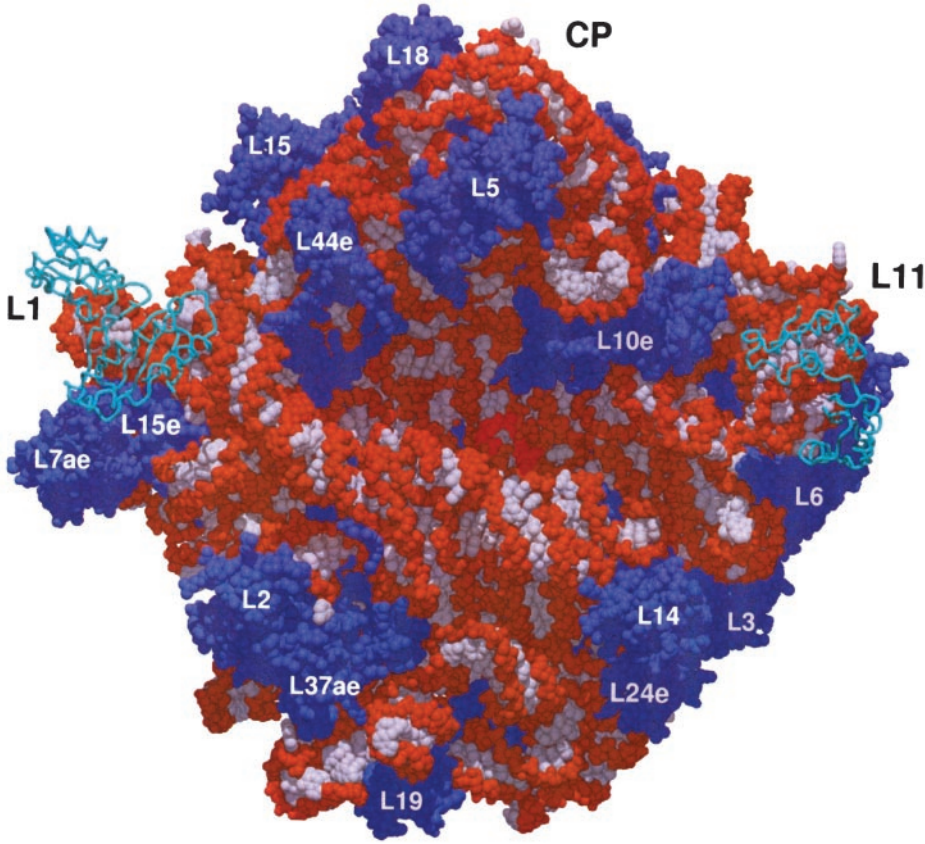

Figure 4 A space filling model of the large ribosomal subunit from *H. marismortui* with a transition state analog bound viewed down the active site cleft. Bases are white, the sugar-phosphate backbone is orange, and the substrate analog (in the center) is red. Proteins whose structures are defined by the 2.4 Å resolution map are blue. Cyan ribbon represents proteins whose structures are independently known that have been positioned approximately using lower resolution electron density maps. Identification numbers are provided for all proteins, and CP designates the central protuberance. [Reproduced with permission from (70).]

more complete analyses have been achieved (72; D. Klein, T.M. Schmeing, P.B. Moore, and T.A. Steitz, in preparation). The major message conveyed is that the primary function of ribosomal proteins is stabilization of rRNA structure, though some are also involved in functionally important interactions with protein factors.

Except for the four proteins that form the tips of the two lateral protuberances, the proteins of the large subunit do not extend significantly beyond the envelope defined by the RNA (Figure 4) (18). Their globular domains are on the exterior

of the particle, often nestled in the gaps and crevices formed by the RNA, thus acting like mortar filling the gaps and cracks between RNA bricks. The distribution of proteins on the subunit surface is nearly uniform, except for the active site cleft and the flat surface that interacts with the 30S subunit, places where they are notably absent.

All of the proteins in the particle, except L12, interact directly with RNA, and all but 7 of the remaining 30 proteins interact with 2 rRNA domains or more (18). Protein L22 interacts with RNA sequences belonging to all six domains of 23S rRNA. About one third of the average protein surface area becomes buried when the subunit forms from its isolated but fully structured components, an average of 3000 $Å^2$ of protein surface area buried per protein, which is comparable to the 2,700 $Å^2$ of glutaminyl-tRNA synthetase that interacts with $tRNA^{Gln}$. Presumably, this enormous contact surface area is essential to energetically compensate for the considerable conformational entropy associated with both a flexible rRNA and the protein tails, which is lost upon subunit assembly.

Unlike proteins that bind to specific DNA sequences, the majority of ribosomal proteins bind to specific locations by recognizing unique RNA shapes through interactions largely with the sugar phosphate backbone rather than through interactions with bases via the major or minor grooves. Proteins that share sequence and structural homology, such as L15 and L18e, interact with their RNA targets in very similar ways. However, unrelated proteins that contain similar structural motifs, such as the RRM-like folds or SH3-like barrels, interact with rRNA in unrelated ways (D. Klein, T.M. Schmeing, P.B. Moore, and T.A. Steitz, in preparation).

PROTEIN TAILS Of all the interactions between ribosomal proteins and the rRNA, the interactions between extended protein tails that penetrate into the interior of the ribosome and the forest of RNA helices are the most unprecedented and the biggest surprise in the *H. marismortui* large subunit structure. At the time the first atomic resolution crystal structures appeared for ribosomes, the structures of a large number of ribosomal proteins in isolation had been established (73); it was anticipated that the conformations of those proteins in the ribosome would be similar to their conformations in isolation, which turned out to be true. What almost no one anticipated (72a) was that the ribosomal proteins that had resisted structure determination contain sequences whose conformations are determined entirely by their interactions with ribosomal RNA, i.e., tails. The *H. marismortui* large subunit includes 12 such proteins (18). In the intact subunit, their globular domains, like the globular domains that constitute the totality of nontailed ribosomal proteins, are found on the surface of the particle, and their tails insert into the ribosome's interior making numerous, idiosyncratic interactions with the surrounding RNA. While being only 18% of the total large subunit protein, they constitute 44% of the total rRNA interaction surface (D. Klein, T.M. Schmeing, P.B. Moore, and T. A. Steitz, in preparation).

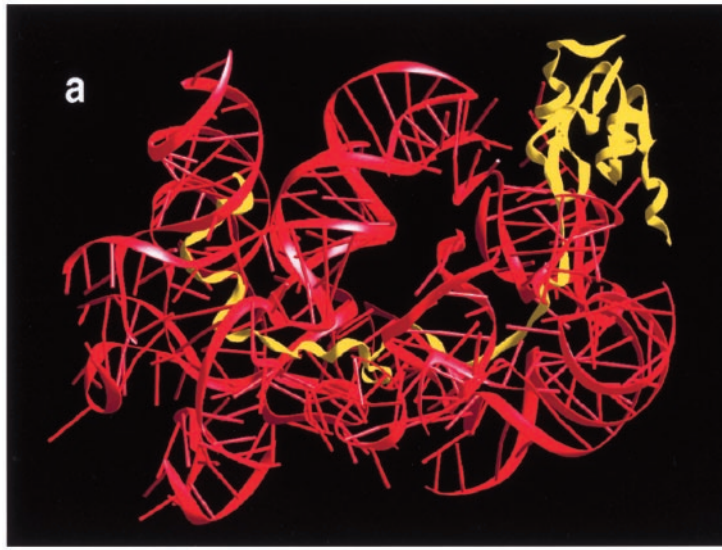

Figure 5 Ribosomal proteins in the *H. marismortui* large ribosomal subunit. (*a*) A ribbon representation of L15 (yellow) and the RNA sequences with which it interacts (red). The globular domain of the protein is exposed to solvent on the surface of the ribosome, but its extended tail penetrates deeply into the subunit. (*b*, *c*) A space-filling representation of proteins in the *H. marismortui* large ribosomal subunit, with the RNA removed, color-coded to display electrostatic charge potential. Negative regions are red, positive regions are blue, and neutral regions are white. The ribosome is seen in the crown view in (*b*), and rotated 180° about its vertical axis in (*c*). The surface of the globular domains of those proteins that face the exterior are acidic, but the surfaces that face the interior, including their tails, are basic (D. Klein, T.M. Schmeing, P.B. Moore, and T.A. Steitz, in preparation).

In many respects, the tails of the ribosomal proteins are reminiscent of those highly basic termini of histone proteins, which also interact with nucleic acid (73a). In all species, the tails of ribosomal proteins are highly basic being about one quarter arginine plus lysine, which makes them suitable for stabilizing the structure of a polyanion like RNA (D. Klein, T.M. Schmeing, P.B. Moore, and T.A. Steitz, in preparation). However, they are not just high mol wt counterions. They also contain an abundance of glycines and prolines, and their sequences are more conserved (20% in archaea and eukaryotes) than those of the globular domains (10%) to which they are attached. Further, the interactions they make with the RNAs surrounding them are highly specific (D. Klein, T.M. Schmeing, P.B. Moore, and T.A. Steitz, in preparation). Because the globular domains of these proteins are acidic, there is a striking segregation of protein charge in the large subunit from *H. marismortui* (Figure 5*b*) with the surface facing the outside of the particle being negative and that in the interior being positive.

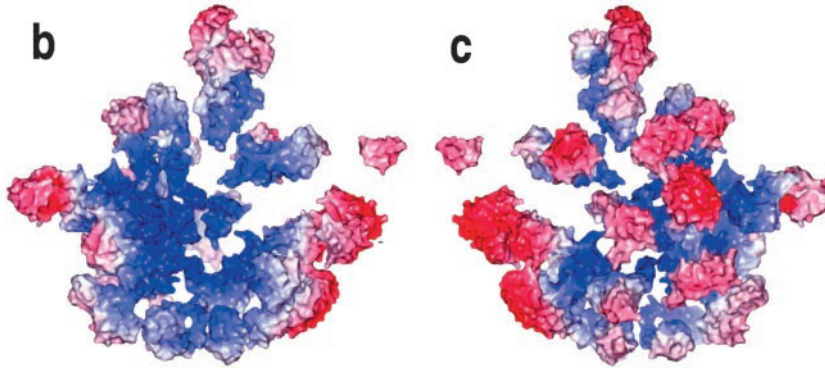

Figure 5 Continued

Examination of the pathway of these protein extensions in and among the spaces between RNA helices suggests that the assembly of the ribosomal RNA and proteins must be a complex, ordered, and cooperative process (Figure 5*a*). Clearly, these tails do not thread their way into the RNA after it has reached its final conformation, but rather must cofold with the RNA. One attractive hypothesis is that the globular domains first interact with a contiguous piece of 23S rRNA, burying more than 1000 $Å^2$ of surface, and then other more remote RNAs cofold around the tails burying significantly smaller surface areas (D. Klein, T.M. Schmeing, P.B. Moore, and T.A. Steitz, in preparation). Indeed, each of the tailed proteins has a single large surface on its globular domain that interacts with a contiguous rRNA structure.

LARGE SUBUNIT ASSEMBLY In the 1960s and 1970s, it was discovered that both prokaryotic ribosomal subunits can be reconstituted in vitro from their isolated components (74, 75). The studies of reconstitution that followed produced most of what is known about the details of ribosome assembly. The general conclusion that emerges when reconstitution data are compared with subunit structures is that the primary function of small subunit proteins is stabilization of 16S rRNA domains, whereas the primary function of large subunit proteins is stabilization of interdomain interactions.

One way to document this difference is to count the number of rRNA domains with which each ribosomal protein makes more than incidental contact. The average for the 30S proteins in *T. thermophilus* is 1.2 per protein (72), while the corresponding average for the 50S protein in *H. marismortui* is 2.3 per protein (18). The large subunit average is skewed because it includes the contributions of L1, L10, L11, and L12, which are components of its two lateral protuberances and do not function in stabilization of the structure. Leaving them out, the average for the large subunit rises to 2.6 different domains contacted per protein.

The interdomain character of large subunit protein/RNA interactions becomes manifest also when large subunit proteins are allowed to interact with isolated 23S rRNA domains (60). The nucleoproteins formed when the 6 23S rRNA domains interact with total large subunit protein one at a time include only 17 of the 32 proteins in the *Escherichia coli* large ribosomal subunit, but another 5 bind when RNAs that include pairs of domains are tested. In contrast, 16 of the 20 small subunit proteins tested associate with isolated 16S rRNA domains (77–79).

It is hard to make detailed comparisons between the experimental reconstitution assembly data available for the large subunit and the structure of the large ribosomal subunit from *H. marismortui* because the assembly data were obtained using *E. coli* ribosomes, and only 20 *H. marismortui* large ribosomal subunit proteins have *E. coli* equivalents. There are some interesting correlations, however. The reconstitution process of Nierhaus and coworkers generates two intermediate ribonucleoproteins, the earlier one is called $RI_{50}(1)$ and the later one called $RI_{50}(2)$ (80). Proteins in *E. coli* that have *H. marismortui* homologues tend to add to assembling subunits early. Of the 21 proteins found in the $RI_{50}(1)$ intermediate, 16 have homologues in *H. marismortui*, but only 6 of the 10 proteins found in the $RI_{50}(2)$ (in addition to the 21 that are already there) have *H. marismortui* homologues. In addition, 5 of the 6 proteins identified as essential for $RI_{50}(1)$ formation have homologues in *H. marismortui*. These observations suggest that the proteins that have homologues in all kingdoms are somehow more important than those that do not.

It is also the case that tailed large subunit proteins are likely to be involved in the early stages of assembly. Eight of the 20 proteins in the homologous set have tails, and all of them are found in the $RI_{50}(1)$ complex. Moreover, of the subset of the proteins essential for the formation of the $RI_{50}(1)$ intermediate that have *H. marismortui* equivalents, 4 out of 5 have tails. This correlation makes structural sense because it is very difficult to understand how protein tails could get inserted into the interior of the RNA core of the subunit once it attains its fully folded form. Tailed proteins ought to join the large subunit early.

THE STRUCTURAL BASIS OF LARGE SUBUNIT ACTIVITY

The most significant result to emerge from the crystal structures of the large ribosomal subunit and its substrate complexes is the finding that the ribosome is a ribozyme. All of the components of the ribosome involved in orienting both the A-site α-amino group and the P-site bound carbonyl carbon it is to attack are made of RNA, as is the rest of the peptidyl transferase center (70). Although proteins do contact ribosome-bound tRNAs and undoubtedly help orient them, the catalytic business of the ribosome is conducted entirely by RNA.

Investigating the Enzymatic Activity of the Peptidyl Transferase Center

The process catalyzed by the peptidyl transferase center of the ribosome is the aminolysis of an ester bond. The nucleophilic α-amino group of an aminoacyl-tRNA bound to the A site of the peptidyl transferase center attacks the carbonyl carbon of the ester bond linking the peptide moiety of a peptidyl-tRNA bound to the P site of the peptidyl transferase center. The anionic, tetrahedral intermediate that results breaks down to yield a deacylated tRNA in the P site and an A-site bound tRNA joined by an ester bond to a peptide that has been extended by one amino acid.

At present, only the structures of 50S ribosomal subunits have been established at sufficiently high resolution to enable a detailed analysis of the peptide bond forming process. The 5.5 Å resolution maps of the 70S ribosome with A- and P-site tRNAs bound do not allow an atomic interpretation of the catalytic site. Although full tRNA molecules are too large to bind in 50S subunit crystals, the 50S subunit will catalyze the formation of a peptide bond using substrate analogues that are fragments of the CCA acceptor ends of tRNA (Figure 6) in what is termed "the fragment reaction" (81, 82), and these fragments do bind to crystals. Puromycin, which is a di-methylated adenosine aminoacylated with a hydroxymethyl tyrosine, is an acceptable A-site substrate, though either C-puromycin or C-C-puromycin is better; molecules as small a CCA aminoacylated with N-formyl methionine will serve as P-site substrates.

All of the published structures of large subunits with substrate, intermediate, and product analogues bound have been obtained using crystals of *H. marismortui* subunits. Not only do fragment substrates diffuse into these crystals and bind, but these subunits will make peptide bonds *in crystalo* (83). Separate structures have been obtained of the large subunit complexed with an A-site fragment substrate, a P-site fragment substrate, and with products bound together in one complex (Figure 7), as well as a complex with an intermediate analogue (70, 83, 84). These structures have been combined to produce a movie showing how the peptide bond forming process could occur on the large subunit (Figure 8) (84). A model of the peptidyl transferase center with both its A site and its P site occupied by substrate analogues (Figure 8*a*) was generated by superimposing the structure of the large subunit with a P-site substrate bound on the independently determined structure of the large subunit with the A site occupied. Because these crystals are enzymatically active and because the activity of the *H. marismortui* subunit in solution is independent of salt concentration and cation identity (83), these structures are likely to be relevant to understanding peptide bond formation by the large subunit.

THE CATALYSIS OF PEPTIDE BOND FORMATION BY THE LARGE RIBOSOMAL SUBUNIT

The structures of these complexes as a group not only prove that the peptidyl transferase site is entirely composed of 23S rRNA, they also provide insight into

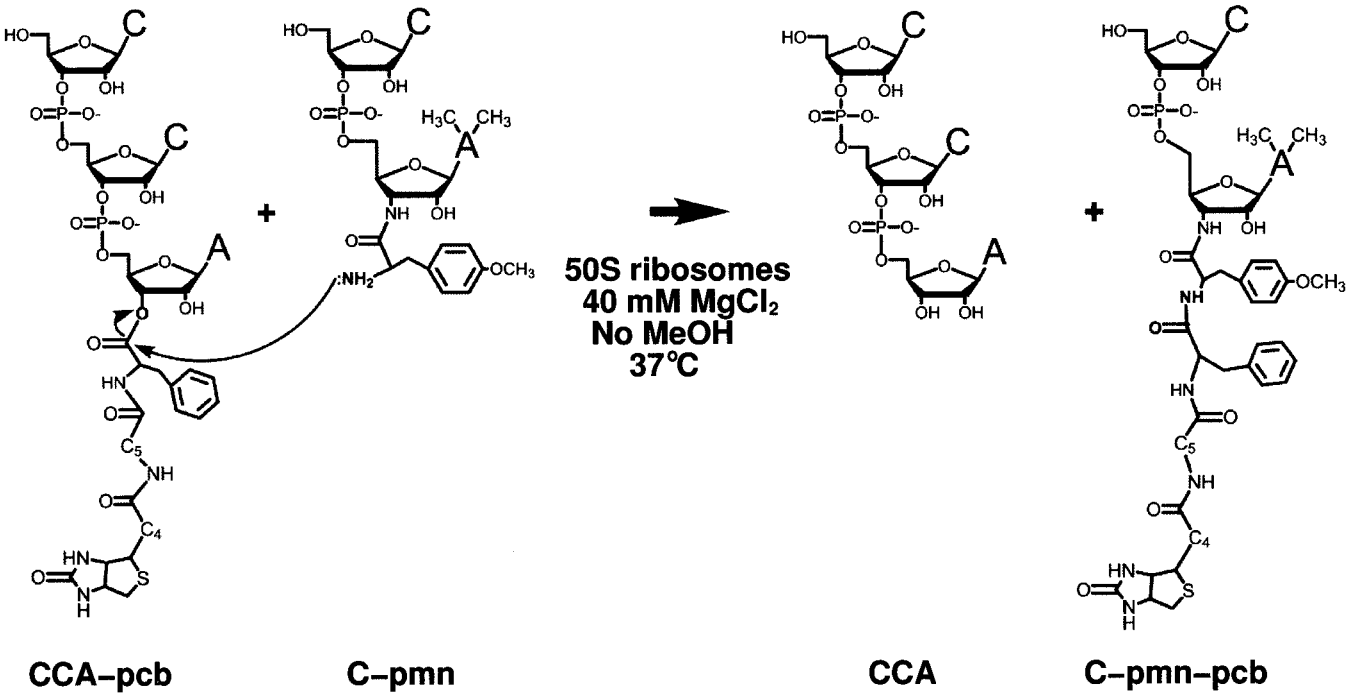

Figure 6 A ribosome-catalyzed peptide bond forming reaction involving low mol wt substrates. The reaction of CCA-phenylalanine-caproic acid-biotin (CCA-pcb) and C-puromycin (C-pmn) that yields CCA and C-puromycin-phenylalanine-caproic acid-biotin (C-pmn-pcb) is catalyzed by large ribosomal subunits. Reactions of this type are analogous to the peptidyl transferase reaction, which occurs on intact ribosomes in vivo and is referred to as the "fragment reaction," because its substrates resemble the 3′ termini of aminoacyl and peptidyl tRNAs. [Reproduced with permission from (83).]

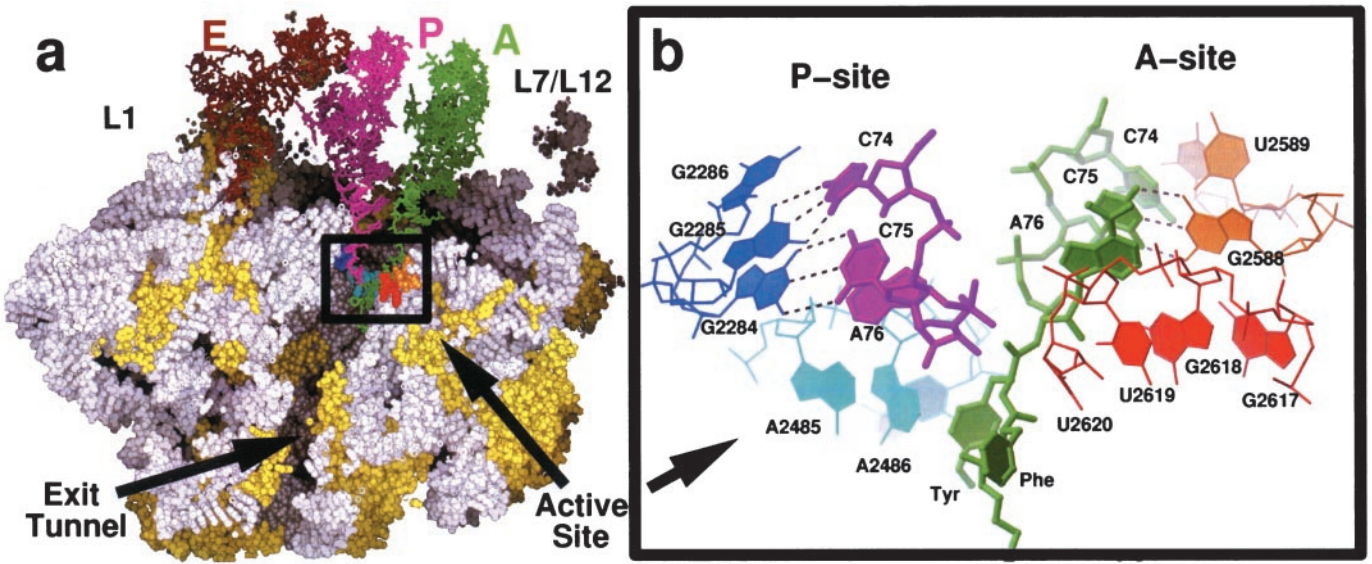

Figure 7 The structure of the large ribosomal subunit from *H. marismortui* with products of the fragment reaction (CCA and C-pmn-pcb: see Figure 6) bound in the peptidyl transferase center. (*a*) A space-filling representation of the complex with three intact tRNAs added in the positions tRNAs assume when bound to the A, P, and E sites of the 70S ribosome (22). rRNA is white, and ribosomal proteins are yellow. The subunit, which is oriented in the crown view, has been cut in half along a plane that passes through the peptide exit tunnel, and the front of the structure has been removed to expose the tunnel lumen. The active site area is in a box. (*b*) A close-up of the active site showing the peptidyl product (CC-pmn-pcb; green) bound to the A-loop (orange), and the deacylated product (CCA; violet) bound to the P-loop (dark blue). The N3 of A2486 (A2451 in *E. coli*) (light blue) is close to the 3′ OH of the CCA, and the base of U2620 (U2585) (red) has moved close to the new peptide bond and the 3′ OH of A76. [Reproduced with permission from (83).]

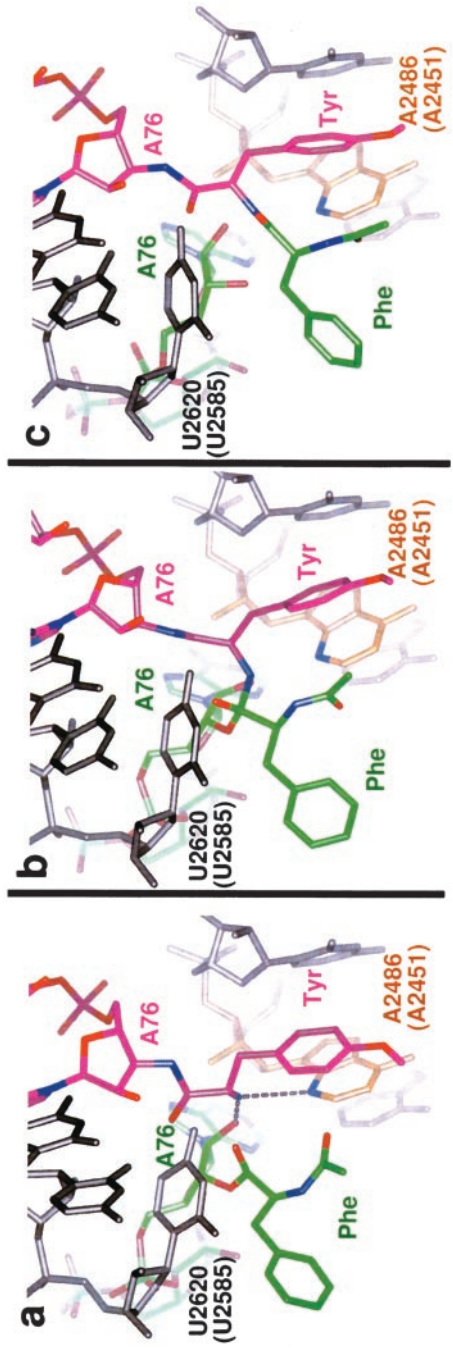

Figure 8 Steps in the peptidyl transferase reaction pathway. (*a*) The superposition of two independently determined cocrystal structures suggests that the α-amino group of an A-site substrate is positioned for a pro-R attack on the carbonyl carbon of the ester bond of the P-site substrate (green). (*b*) A model for the tetrahedral intermediate that would result if the reaction were to occur in the manner suggested by Figure 8*a*. Note that the oxyanion points away from A2486 (2451). (*c*) The structure of the products of the the peptidyl transferase reaction bound to the peptidyl transferase center. [Reproduced with permission from (84).]

the ways the large subunit facilitates peptide bond formation. Of primary importance for the catalytic activity of the peptidyl transferase center is the proper alignment of substrates, as is the case for all enzymes (70, 85, 86). It is clear that the peptidyl transferase center, including the A- and P-loops and A2486 (2451), is organized to bring the nucleophilic α-amino group of an A-site aminoacyl-tRNA into contact with the carbonyl carbon with which it reacts during peptide bond formation (Figure 8*a*).

We still do not know the extent to which, or how, the peptidyl transferase center also chemically enhances the rate of peptide bond formation. There is no evidence for metal ion involvement, although until a structure is obtained with substrates bound to both the A site and the P site simultaneously, metal ion involvement will be difficult to exclude. In the present model for A-site and P-site substrates bound to the center there are, however, three rRNA groups close enough to the reaction site to form hydrogen bonds with the reactive α-amino group: (1) the 2′ OH of A76 of the tRNA in the P site, (2) the N3 of A2486 (A2451 in *E. coli*5) of 23S rRNA, and (3) the 2′ OH of A2486 (2451) (84). These hydrogen bonds must help align the α-amino group, and there is reason to believe that hydrogen bond formation alone may enhance reactivity by several orders of magnitude beyond what it contributes to alignment (86a). If any of these groups were in addition to have an elevated pK_a, its hydrogen bonding interactions could further accelerate the rate of peptide bond formation by enhancing the nucleophilicity of the α-amino group.

Nothing is known about the role of the 2′ OH of A2486 (2451) in protein synthesis. However, tRNAs that terminate with a 2′ deoxyadenosine can be aminoacylated and are A-site substrates, but 2′deoxy-A76 peptidyl tRNAs are inactive as P-site substrates (87). The 2′OHs of A76 of tRNAs bound in the P site are thus likely to be important for A-site substrate alignment, but a more active role for them cannot be ruled out.

Many experiments have been done to test the proposal that the N3 of A2486 (2451) enhances the rate of peptide bond formation chemically by general acid/base catalysis and intermediate stabilization (70, 88). Two important points about that hypothesis have now been clarified. First, present structural data indicate that A2486 is unlikely to help stabilize the oxyanion intermediate (84) because the anionic oxygen of the tetrahedral intermediate constructed from the substrate complexes appears to point away from the N3 of A2486 (2451) (Figure 8*b*). Second, contrary to earlier reports (89, 91–93), mutation of A2486 (2451) to U reduces the rate of the chemical step of peptide bond formation in 70S ribosomes by about 100-fold at basic pHs. Furthermore, the A2486 (2451)-associated rate effect titrates with a pK_a of about 7.5 (94). These observations are compatible with the hypothesis that the N3 of A2486 has a pK_a of 7.5 (but see 90), and activates the α-amino group as a general base (70). A more indirect hypothesis that the peptidyl transferase center is activated by a pH-dependent conformational change that for some unknown reason depends on the identity of

the base at position 2486 (2451) is also consistent with these kinetic data (94). Further experimentation will be required to settle these issues.

THE LARGE SUBUNIT-CATALYZED PEPTIDE BOND FORMATION AS A MODEL FOR PEPTIDE BOND FORMATION Most of the statements about the chemistry of peptide bond formation found in textbooks today derive from studies of large subunit catalyzed fragment reactions like those just described. There are reasons for believing the fragment reaction is biologically relevant. First, both the 70S ribosome and the 50S subunit promote the reaction of the same low mol wt substrates. Second, the substrates and products of the fragment reaction are obviously related to those of the normal protein synthesizing system. Third, the fragment reaction and the normal peptidyl transferase reaction occur at the same site in the large ribosomal subunit. Fourth, both reactions are sensitive to many of the same inhibitors.

However, it appears that the full peptidyl transferase reaction catalyzed by the 70S ribosome may have additional catalytically important features, since its rate is about 10^4 times faster. At 37°C, bacteria synthesize protein at a rate of about 20 amino acids per second (95), and the rate of the chemical, bond-forming step in that sequence of reactions is probably $>100\ s^{-1}$ (96). Consistent with this estimate, under saturating substrate conditions, puromycin will react with peptidyl tRNA bound to mRNA-programmed 70S ribosomes at a rate of $\sim 70\ s^{-1}$ (94), which is 3 to 4 orders of magnitude faster than 50S subunits catalyze the reaction of puromycin with low mol wt P-site substrates (97). This rate difference may mean that the peptidyl transferase center in reaction-ready 70S ribosomes has a configuration that differs from that seen in the large ribosomal subunit, although the structural differences are likely to be modest. Alignment of the *H. marismortui* 50S structure and that from the 70S shows that the A- and P-site tRNAs bound to the 70S ribosome can connect smoothly with the fragment substrates bound to the 50S subunit (84). However, the low resolution of the 70S ribosome study (22) cannot exclude (or support) a small, but catalytically important, alteration in the presentation of the nucleophilic 5 α-amino group to the carbonyl group it attacks or in its relationship to surrounding ribosomal groups.

The Polypeptide Exit Tunnel

The polypeptide exit tunnel of the large subunit is a passage about 100 Å long that begins immediately below the peptidyl transferase center, and ends at the back side of the large subunit (Figure 7*a*). Most nascent proteins pass though the tunnel as they are synthesized, but there is evidence that at least some can leave the ribosome by other routes [reviewed in (98)]. The signal recognition particle (SRP), which recognizes the signal sequences of proteins destined to be inserted into membranes or secreted through them, interacts with those sequences when they reach the distal end of the tunnel. The SRP also interacts with proteins that

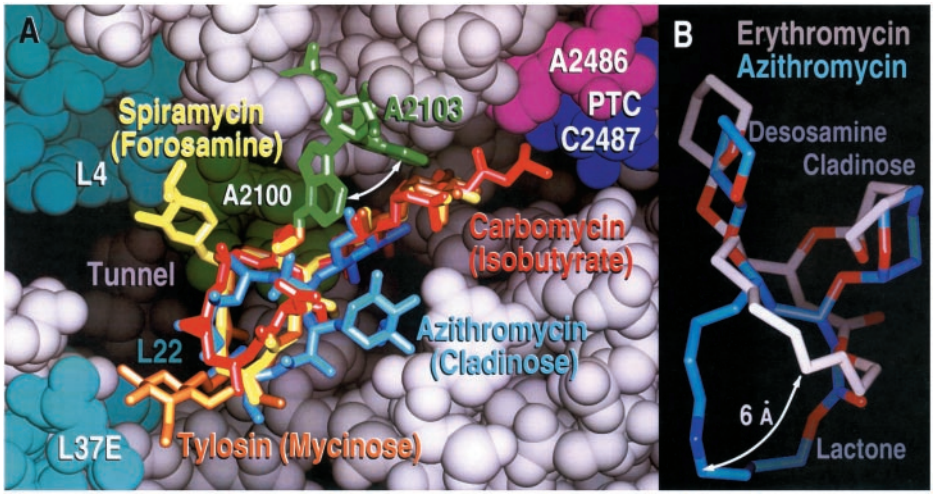

Figure 9 The interaction of macrolide antibiotics with the large ribosomal subunit of *H. marismortui*. (*a*) A superposition of several macrolides/large ribosomal subunit complex structures. Structures containing carbomycin (red), tylosin (orange), spiramycin (yellow), and azithromycin (blue) have been superimposed by aligning corresponding 23S rRNA atoms in four independently determined crystal structures. The macrolide rings of the four antibiotics bind to virtually the same site in the proximal portion of the peptide exit tunnel. In the case of the 16-membered macrolides examined (tylosin, carbomycin, and spiramycin), A2103 (2062) swings down so that its N6 can form a covalent bond with their aldehyde substituents. The differences between these drugs are due primarily to the substitutents on their macrolide rings, which differ in chemical nature, bulk, and placement. Some extend into the peptidyl transferase center. (*b*) The position assumed by erythromycin (white) when bound to the large ribosomal subunit from *D. radiodurans* (104) compared to that adopted by azithromycin (blue) bound to the large ribosomal subunit from *H. marismortui*. [Reproduced with permission from (105).]

surround the end of the tunnel (100). By a mechanism that is not fully understood but may involve interaction of the SRP with the factor binding site, the interaction of a ribosome engaged in the synthesis of such a protein with a SRP prevents it from completing the synthesis of that protein until it has become membrane bound in association with a translocon, the pore structure through which the protein must pass (101).

The wall of the tunnel is formed entirely by RNA for the first third of its length extending from the PTC to a constriction that is formed by portions of ribosomal proteins L4 and L22, which are highly conserved components of the ribosome. Below the constriction, the bore of the tunnel becomes large enough to accommodate an α-helix, and below the point where L39e contributes sequences to its wall, it becomes even wider. Electron microscopists claim that the tunnel

bifurcates in its lower reaches, and hence that there are two ways for nascent polypeptides to exit from the ribosome (10). This feature of the tunnel is not confirmed by the atomic resolution crystal structures (70). The appearance of a side tunnel in the EM may be a resolution artifact, which results from Fourier series termination effects; a feature in the crystal structure that may appear as a side tunnel in the EM is in fact completely occluded by protein. There is only one passage big enough to accept a polypeptide that passes through the large subunit.

The tunnel, of course, has to allow the passage of nascent proteins of all sequences, and hence its wall ought to possess a nonstick character. Indeed, consistent with this expectation, its wall is a mosaic of small hydrophobic and hydrophilic patches, which for most of the tunnel appear to be too small to promote strong interactions with nascent peptides (18). A possible exception is the upper part of the tunnel near the PTC where two bases splay apart at two locations and form binding sites for antibiotics (105). Furthermore, there are some short hydrophobic peptide sequences that appear to stick to the tunnel, presumably near the PTC, and function in the regulation of translation (98, 102). It is possible that these regulatory peptide sequences and some antibiotics exploit the same binding opportunities. Sequences that stick in the tunnel have probably been selected against for the vast majority of proteins.

One of the most intriguing unanswered questions about the tunnel is how nascent polypeptides proceed down its lumen: Is it a passive diffusion process or are there shape changes that occur in the tunnel during protein synthesis that actively promote the passage of nascent polypeptides? The conformation of the tunnel is indistinguishable in the two 50S structures and the 70S structure as well as all of the substrate analogue and antibiotic complexes established thus far, which implies that the process may be passive. However, Frank and coworkers (103, 103a) have proposed that the tunnel functions like a peristaltic pump to facilitate the passage of peptides. They report large differences in the tunnel diameter between wild-type ribosomes and ribosomes possessing mutations in either protein L4 or L22 that render these ribosomes resistant to macrolides. It will be of interest to see in an atomic structure how such shape changes can be

Figure 10 Antibiotic structures and antibiotic interactions with the *H. marismortui* large ribosomal subunit. (*a*) The structures of two macrolide antibiotics. (*b*) The interactions of sparsomycin (green), puromycin (red), blasticidin S (magenta), chloramphenicol (light blue), carbomycin (dark blue), and streptogramin A (blue) with the large ribosomal subunit. The ribosome has been split open as in Figure 7*a* to reveal the lumen of the exit tunnel and adjacent regions of the peptidyl transferase site. Ribosomal components are depicted as a continuous surface. Seven independently determined cocrystal structures have been aligned by superimposing the 23S rRNA in each complex. The sites to which these antibiotics bind are all different, but there is extensive overlap (J. Hansen, P.B. Moore, and T.A. Steitz, manuscript in preparation).

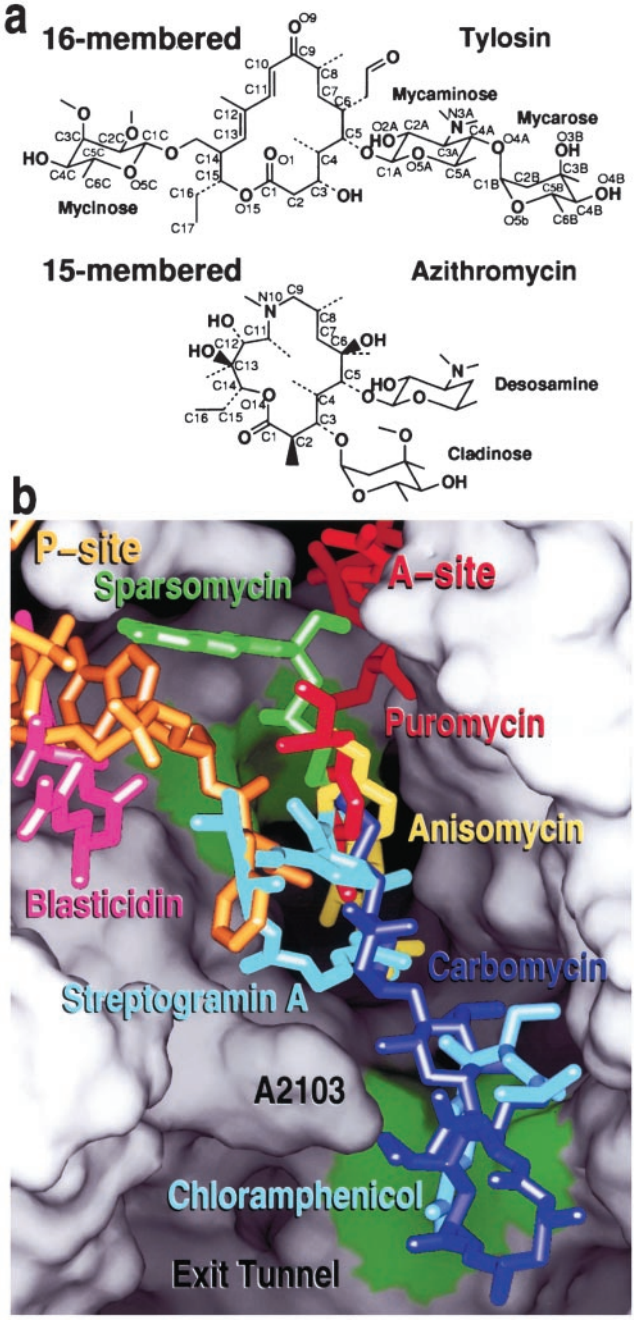
a
16-membered
Tylosin
Mycaminose
Mycarose
Mycinose
15-membered
Azithromycin
Desosamine
Cladinose
b
P–site
Sparsomycin
A–site
Puromycin
Anisomycin
Blasticidin
Carbomycin
Streptogramin A
A2103
Chloramphenicol
Exit Tunnel

achieved and whether or not they might be related normal functions of the native ribosome.

Antibiotics Targeting the Large Subunit

For the biochemical community interested in antibiotics that block ribosome function, the last two years have been one long field day in which a wealth of information on the structures of antibiotic complexes of both the large and small subunit has been published. The structures of five different antibiotic complexes with the *D. radiodurans* large subunit were established: chloramphenicol, clindamycin, and the 14-membered macrolides (erythromycin, clarithromycin, and roxithromycin) (104). Complexes of the *H. marismortui* large subunit with the 16-membered macrolides (tylosin, carbomycin, and spiramycin), as well as the 15-membered macrolide, azithromycin, (105), and complexes of the *H. marismortui* large subunit with the nonmacrolide antibiotics (anisomysin, blasticidin, sparsomycin, virginiamycin M, and chloramphenicol) bound to a second site have all been determined (J.L. Hansen, P.B. Moore, and T.A. Steitz, unpublished observations).

All of the macrolide antibiotics bind in largely the same place in the proximal part of polypeptide exit tunnel adjacent to the peptidyl transferase center and before the constriction formed by L4 and L22 (Figure 9). They all appear to inhibit protein syntheses by blocking the passage of nascent peptides down the tunnel or, as in the case of carbomycin A, by inhibiting A-site substrate binding. The saccharide branch attached to C5 of the lactone rings extends toward the PTC, and the isobuterate extension of the carbomycin A dissaccharide overlaps the A site. In the case of the 16-membered macrolides, a reversible covalent bond forms between the ethyladehyde substituent at the C6 position and the N6 of A2063 (A2062, *E. coli*). The orientation of the 14-membered lactose rings of the macrolides bound to the eubacteria *D. radiodurans* large subunit differs significantly from that of the 15- and 16-membered lactose rings bound to the archaeal *H. marismortui* large subunit. Whether this is due to a difference between the binding of 14-membered and the 15- or 16-membered macrolides or due to a difference between eubacteria and archaea, such as occurs at position 2058 in 23S RNA, is not yet established. Interactions of all seven macrolides with the large subunit seen in the structures are consistent with prior biochemical and genetic data.

The structures of seven nonmacrolide antibiotics complexed with either the *H. marismortui* or the *D. radiodurans* large subunit show that these compounds bind to sites that overlap those of either peptidyl tRNA or aminoacyl-tRNA, consistent with their functioning as competitive inhibitors of peptide bond formation (104; J.L. Hansen, P.B. Moore, and T.A. Steitz, in preparation). One hydrophobic crevice in the PTC forms the binding site for a tyrosine side chain of A-site analogues as well as for anisomycin and chloramphenicol. Sparsomycin interacts primarily with a P-site bound substrate but also extends into the active site hydrophobic crevice just mentioned, as does the isobuterate extension of the

carbomycin A dissaccharide. Virginiamycin M occupies portions of both the A site and P site, and it induces a conformational change in A2103, while blasticidin S exploits another strategy by mimicking C74 and C75 of a P-site bound tRNA and base pairing with the P-loop.

Many of these antibiotics bind in nearby but, in some cases, nonoverlapping sites (Figure 10), which suggests a strategy for the design of new antibiotics that may overcome many known antibiotic resistance mutations. One could imagine synthesizing hybrid antibiotics by combining portions of two antibiotics that bind adjacent sites. In any case, these structures provide important leads for the design and synthesis of new antibiotics that target the large ribosomal subunit. Thus, it is now possible to use the same structure based drug design approach that was so successful with HIV protease to design novel antibiotics targeting the large ribosomal subunit, in spite of its being 100 times larger than the protease.

ACKNOWLEDGMENTS

We thank Nenad Ban, Jeff Hansen, Joe Ippolito, Dan Klein, Poul Nissen, and Martin Schmeing. This research was supported by NIH grant GM22778 and an Agouron Institute grant to P.B.M. and T.A.S.

The *Annual Review of Biochemistry* is online at http://biochem.annualreviews.org

LITERATURE CITED

1. Robertus JD, Ladner JE, Finch JT, Rhodes D, Brown RS, et al. 1974. *Nature* 250:546–51
2. Kim SH, Suddath FL, Quigley G, McPherson A, Sussman JL, et al. 1974. *Science* 185:435–40
3. Rheinberger H-J, Geigenmuller U, Gnirke A, Hausner T-P, Remmer J, et al. 1990. In *The Ribosome*, ed. WE Hill, AE Dahlberg, RA Garrett, PB Moore, D Schlessigner, JR Warner, pp. 318–30. Washington, DC: Am. Soc. Microbiol.
4. Lake JA. 1976. *J. Mol. Biol.* 105:131–59
5. Stoeffler G, Stoeffler-Meilicke M. 1984. *Annu. Rev. Biophys. Bioeng.* 13:303–30
6. Shatsky IN, Evstafieva AG, Bystrova TF, Bogdanov AA, Vasiliev VD. 1980. *FEBS Lett.* 121:97–100
7. Oakes M, Henderson E, Scheinman A, Clark M, Lake JA. 1986. See Ref. 106, pp. 47–67
8. Stoeffler G, Stoeffler-Meilicke M. 1986. See Ref. 106, pp. 28–46
9. Stark H, Mueller F, Orlova EV, Schatz M, Dube P, et al. 1995. *Structure* 3:815–21
10. Frank J, Zhu J, Penczek P, Li YH, Srivastava S, et al. 1995. *Nature* 376: 441–44
11. Bernabeu C, Lake JA. 1982. *Proc. Natl. Acad. Sci. USA* 79:3111–15
12. Bernabeu C, Tobin EM, Fowler A, Zabin I, Lake JA. 1983. *J. Cell Biol.* 96:1471–74
13. Milligan RA, Unwin PNT. 1986. *Nature* 319:693–95

13a. Yonath A, Leonard KR, Wittmann HG. 1987. *Science* 236:813–16

14. Stark H, Orlova EV, Rinke-Appel J, Junke N, Mueller F, et al. 1997. *Cell* 88:19–28

15. Stark H, Rodnina MV, Rinke-Appel J, Brimacombe R, Wintermeyer W, van Heel M. 1997. *Nature* 389:403–6
16. Agrawal RK, Penczek P, Grassucci RA, Li YH, Leith A, et al. 1996. *Science* 271:1000–2
17. Agrawal RK, Penczek P, Grassucci RA, Frank J. 1998. *Proc. Natl. Acad. Sci. USA* 95:6134–38
18. Ban N, Nissen P, Hansen J, Moore PB, Steitz TA. 2000. *Science* 289:905–20
19. Wimberly BT, Brodersen DE, Clemons WM, Morgan-Warren RJ, Carter AP, et al. 2000. *Nature* 407:327–39
20. Pioletti M, Schlunzen F, Harms J, Zarivach R, Glühmann M, et al. 2001. *EMBO J.* 20:1829–39
21. Harms J, Schluenzen F, Zarivach R, Bashan A, Gat S, et al. 2001. *Cell* 107:679–88
22. Yusupov MM, Yusupova GZ, Baucom A, Lieberman K, Earnest TN, et al. 2001. *Science* 292:883–96
23. Yonath A. 2002. *Annu. Rev. Biophys. Biomol. Struct.* 31:257–73
24. Ramakrishnan V. 2002. *Cell* 108:557–72
25. Ramakrishnan V, Moore PB. 2001. *Curr. Opin. Struct. Biol.* 11:144–54
26. Moore PB. 2001. *Biochemistry* 40: 3241–50
27. Moore PB, Steitz TA. 2003. *RNA* 9:155–59
28. Moore PB, Steitz TA. 2002. *Nature* 418:229–35
29. Yonath A, Mussig J, Tesche B, Lorenz S, Erdmann VA, Wittmann HG. 1980. *Biochem. Int.* 1:428–35
30. Trakanov SD, Yusupov MM, Agalarov SC, Garber MB, Ryazantsev SN, et al. 1987. *FEBS Lett.* 220:319–22
31. Glotz C, Mussig J, Gewitz HS, Makowski I, Arad T, et al. 1987. *Biochem. Int.* 15:953–60
32. Yusupov MM, Tichenko SV, Trakanov SD, Ryazantsev SN, Garber MB. 1988. *FEBS Lett.* 238:113–15
33. Yonath A, Glotz C, Gewitz HS, Bartels H, von Bohlen K, et al. 1988. *J. Mol. Biol.* 203:831–34
34. Shoham M, Wittmann HG, Yonath A. 1987. *J. Mol. Biol.* 193:819–22
35. von Bohlen K, Makowski I, Hansen HAS, Bartels H, Berkovitch-Yellin Z, et al. 1991. *J. Mol. Biol.* 222:11–15
36. Yonath A, Franceschi F. 1998. *Structure* 6:679–84
37. Harms J, Tocilj A, Levin I, Agmon I, Stark H, et al. 1999. *Structure* 7:931–41
38. Ban N, Nissen P, Hansen J, Capel M, Moore PB, Steitz TA. 1999. *Nature* 400:841–47
39. Clemons WMJ, Brodersen DE, McCutcheon JP, May JLC, Carter AP, et al. 2001. *J. Mol. Biol.* 310:827–43
40. Schluenzen F, Tocilj A, Zarivach R, Harms J, Gluehmann M, et al. 2000. *Cell* 102:615–23
40a. Haas DJ, Rossmann MG. 1970. *Acta Crystallogr. B* 26:998–1004
40b. Hope H. 1988. *Acta Crystallogr. B* 44:22–26
41. Hope H, Frolow F, von Bohlen K, Makowski I, Kratky C, et al. 1989. *Acta Crystallogr. B* 45:190–99
42. Jack A, Harrison SC, Crowther RA. 1975. *J. Mol. Biol.* 97:163–72
43. Schlunzen F, Hansen HAS, Thygesen J, Bennett WS, Volkmann N, et al. 1995. *Biochem. Cell Biol.* 73:739–49
44. Yonath A, Harms J, Hansen HAS, Bashan A, Schlunzen F, et al. 1998. *Acta Crystallogr. A* 54:945–55
45. Bashan A, Pioletti M, Bartles H, Janell D, Schlunzen F, et al. 2000. In *The Ribosome*, ed. RA Garrett, S Douthwaite, A Liljas, AT Matheson, PB Moore, HF Noller, pp. 21–33. Washington, DC: Am. Soc. Microbiol. Press
46. Ban N, Freeborn B, Nissen P, Penczek P, Grassucci RA, et al. 1998. *Cell* 93:1105–15
46a. Hansen JL, Schmeing TM, Klein DJ, Ippolito JA, Ban N, et al. 2001. *Cold*

Spring Harbor Symp. Quant. Biol. 66:33–42
46b. Abrahams JP, Leslie AGW. 1996. *Acta Crystallogr. D* 52:30–42
47. Ramakrishnan V, Capel MS, Clemons WM, May JLC, Wimberly BT. 2000. See Ref. 45, pp. 1–10
48. Clemons WM Jr, May JLC, Wimberly BT, McCutcheon JP, Capel MS, Ramakrishnan V. 1999. *Nature* 400: 833–40
49. Deleted in proof
50. Cate JH, Yusupov MM, Yusupova GZ, Earnest TN, Noller HF. 1999. *Science* 285:2095–104
51. Deleted in proof
52. Bashan A, Agmon I, Zarivach R, Schluenzen F, Harms J, et al. 2001. *Cold Spring Harbor Symp. Quant Biol.* 64:43–56
53. Bujnicki JM, Feder M, Rychlewski L, Fischer D. 2002. *FEBS Lett.* 525:174–75
54. Harms J, Schluenzen F, Zarivach R, Bashan A, Bartels H, et al. 2002. *FEBS Lett.* 525:176–78
55. Noller HF, Kop J, Wheaton V, Brosius J, Gutell RR, et al. 1981. *Nucleic Acids Res.* 9:6167–89
56. Cannone JJ, Subramanian S, Schnare MN, Collett JR, D'Souza LM, et al. 2002. *BioMed. Cent. Bioinf.* 3:2
57. Andersen A, Larsen N, Leffers H, Kjems J, Garrett RA. 1986. In *Structure and Dynamics of RNA*, ed. PH Knippenberg, CW Hilbers, pp. 221–37. New York: Plenum
58. Egebjerg J, Leffers H, Christensen A, Andersen H, Garrett RA. 1987. *J. Mol. Biol.* 196:125–36
59. Leffers H, Egebjerg J, Andersen A, Christensen T, Garrett RA. 1988. *J. Mol. Biol.* 204:507–22
60. Ostergaard P, Phan H, Johansen LB, Egebjerg J, Ostergaard L, et al. 1998. *J. Mol. Biol.* 284:227–40
61. Moore PB. 1999. *Annu. Rev. Biochem.* 67:287–300
62. Westhof E, Fritsch V. 2000. *Struct. Fold. Des.* 8:R55–65
63. Klein DJ, Schmeing TM, Moore PB, Steitz TA. 2001. *EMBO J.* 20:4214–21
64. Nagaswamy U, Fox GE. 2002. *RNA* 8:1112–19
65. Szep S, Wang J, Moore PB. 2003. *RNA* 9:44–51
66. Michel F, Westhof E. 1990. *J. Mol. Biol.* 216:585–610
67. Cate J, Gooding AR, Podell E, Zhou K, Golden BL, et al. 1996. *Science* 273: 1678–85
68. Nissen P, Ippolito JA, Ban N, Moore PB, Steitz TA. 2001. *Proc. Natl. Acad. Sci. USA* 98:4899–903
69. Deleted in proof
70. Nissen P, Hansen J, Ban N, Moore PB, Steitz TA. 2000. *Science* 289:920–30
71. Ogle JM, Brodersen DE, Clemons WM, Tarry MJ, Carter AP, Ramakrishnan V. 2001. *Science* 292:897–902
72. Brodersen DE, Clemons WM, Carter AP, Wimberly BT, Ramakrishnan V. 2002. *J. Mol. Biol.* 316:725–68
72a. Liljas A. 1991. *Int. Rev.Cytol.* 124: 103–36
73. Ramakrishnan V, White SW. 1998. *Trends Biochem. Sci.* 23:208–12
73a. Luger K, Mader AW, Richmond RK, Sargent DF, Richmond TJ. 1997. *Nature* 389:251–60
74. Traub P, Nomura M. 1968. *Proc. Natl. Acad. Sci. USA* 59:777–84
75. Nierhaus KH, Dohme F. 1974. *Proc. Natl. Acad. Sci. USA* 71:4713–17
76. Deleted in proof
77. Weitzmann CJ, Cunningham PR, Nurse K, Ofengand J. 1993. *FASEB J.* 7: 177–80
78. Agalarov SC, Selivanova OM, Zheleznyakova EN, Zheleznaya IA, Matvienko NI, Spirin AS. 1999. *Eur. J. Biochem.* 266:533–37
79. Samaha RR, O'Brien B, O'Brien TW, Noller HF. 1994. *Proc. Natl. Acad. Sci. USA* 91:7884–88

80. Herold M, Nierhaus KH. 1987. *J. Biol. Chem.* 262:8826–33
81. Traut RR, Monro RE. 1964. *J. Mol. Biol.* 10:63–72
82. Monro RE. 1967. *J. Mol. Biol.* 26: 147–51
83. Schmeing TM, Seila AC, Hansen JL, Freeborn B, Soukup JK, et al. 2002. *Nat. Struct. Biol.* 9:225–30
84. Hansen JL, Schmeing TM, Moore PB, Steitz TA. 2002. *Proc. Natl. Acad. Sci. USA* 99:11670–75
85. Page MI, Jencks WP. 1971. *Proc. Natl. Acad. Sci. USA* 68:1678–83
86. Nierhaus KH, Schulze H, Cooperman BS. 1980. *Biochem. Int.* 1:185–92
86a. Chamberlin SI, Weeks KM. 2002. *Proc. Natl. Acad. Sci. USA* 99:14688–93
87. Quiggle K, Kumar G, Ott TW, Ryu EK, Chladek S. 1981. *Biochemistry* 20: 3480–85
88. Muth GW, Ortoleva-Donnelly L, Strobel SA. 2000. *Science* 289:947–50
89. Bayfield MA, Dahlberg AE, Schulmeister U, Dorner S, Barta A. 2001. *Proc. Natl. Acad. Sci. USA* 98:10096–101
90. Muth GW, Chen L, Kosek A, Strobel S. 2001. *RNA* 7:1403–15
91. Xiong L, Polacek N, Sander P, Boettger EG, Mankin AS. 2001. *RNA* 7:1365–69
92. Polacek N, Gaynor M, Yassin A, Mankin AS. 2001. *Nature* 411:498–501
93. Thompson J, Kim DF, O'Connor M, Lieberman KR, Bayfield MA, et al. 2001. *Proc. Natl. Acad. Sci. USA* 98:9002–7
94. Katunin VI, Muth GW, Strobel S, Wintermeyer W, Rodnina MV. 2002. *Mol. Cell* 10:339–46
95. Kjeldgaard NO, Gaussing K. 1974. In *Ribosomes*, ed. M Nomura, A Tisseres, P Lengyel, pp. 369–92. Cold Spring Harbor, NY: Cold Spring Harbor Press
96. Rodnina MV, Pape T, Savelsbergh A, Mohr D, Matassova NB, Wintermeyer W. 2000. See Ref. 45, pp. 301–17
97. Maden BEH, Traut RR, Monro RE. 1968. *J. Mol. Biol.* 35:333–45
98. Tenson T, Ehrenberg M. 2002. *Cell* 108:591–94
99. Deleted in proof
100. Pool MR, Stumm J, Fulga TA, Sinning I, Dobberstein B. 2002. *Science* 297: 1345–48
101. Keenan RJ, Freymann DM, Stroud RM, Walter P. 2001. *Annu. Rev. Biochem.* 70:755–75
102. Gong F, Yanofsky C. 2002. *Science* 297:1864–67
103. Frank J, Agrawal RK. 2000. *Nature* 406:318–22
103a. Gabasvili IS, Gregory ST, Valle M, Grassucci R, Worbs M, et al. 2001. *Mol. Cell* 8:181–88
104. Schluenzen F, Zarivach R, Harms J, Bashan A, Tocilj A, et al. 2001. *Nature* 413:814–21
105. Hansen JL, Ban N, Nissen P, Moore PB, Steitz TA. 2002. *Mol. Cell* 10:117–26
106. Hardesty B, Kramer G, eds. 1986. *Structure, Function, and Genetics of Ribosomes.* New York: Springer-Verlag